N79-20064

NASA CR-159024

NUMERICAL PREDICTION OF TURBULENT THREE-DIMENSIONAL JUNCTURE REGION FLOW USING THE PARABOLIC NAVIER-STOKES EQUATIONS

By

A. J. Baker

P. D. Manhardt

&

J. A. Orzechowski

March 1979

Prepared Under Contract NAS1-14307

By

COMPUTATIONAL MECHANICS CONSULTANTS, INC.

3601-A Chapman Highway

Knoxville, Tennessee 37920

For

NASA

National Aeronautics and Space Administration

TABLE OF CONTENTS

NUMERICAL PREDICTION OF TURBULENT THREE-DIMENSIONAL JUNCTURE REGION FLOW USING THE COMOC III 3DPNS COMPUTER PROGRAM

By

A. J. Baker, P. D. Manhardt,

And J. A. Orzechowski

Computational Mechanics Consultants, Inc.

Knoxville, TN 37920

SUMMARY

A numerical solution algorithm is established for prediction of subsonic turbulent three-dimensional flows in aerodynamic configuration juncture regions. In concert with a full three-dimensional exterior potential flow solution, the developed parabolic algorithm yields prediction of the details of the corner region flows. A turbulence closure model is established using the complete Reynolds stress. Pressure coupling is accomplished using the concepts of complementary and particular solutions to a Poisson equation. Numerical results are presented for prediction of the three-dimensional turbulent flow in the juncture of two intersecting parabolic arc airfoils. Specifications for data input juncture geometry modifications are presented.

INTRODUCTION

This effort is in support of the advanced aerodynamics area of the Aircraft Energy Efficiency (ACEE) program. Specifically, a viscous-inviscid flow analysis is required developed and evaluated for prediction of the viscous and turbulence effects in a geometry corresponding to juncture regions of wing-body, pylon-wing, and/or winglet-wing intersections. The effort reported herein focuses on the development and formulation of a method and an associated computer program for calculation of the viscous and turbulent flow in the region of wing-body, pylon-wing, and winglet-wing intersections considering the geometries appropriate to supercritical wing design (including winglets), and the interference effects due to propulsion installation.

The state-of-the-art of three-dimensional boundary-layer calculations has matured to where finite wings as well as bodies can be treated. Prior to the current analysis, no valid technique has been developed which can properly analyze the juncture region of a wing-body combination. This void in analysis capabilities handicaps the designing of aircraft free from flow separation and the evaluating and minimizing of aircraft drag. As a consequence, current three-dimensional boundary-layer programs require inboard starting profiles that must either be obtained from an infinite swept-wing solution or an infinite tapered wing solution, otherwise an assumption of symmetry at the starting line is required. Similar assumptions are required at the tip.

Three-dimensional flows over finite intersecting surfaces fall into two general categories as a function of the flow structure in the plane transverse to its predominant direction. This in turn is strongly dependent on the flow Reynolds number. The essential geometry of the juncture problem corresponds to flow in the immediate vicinity of one corner of a duct, see Figure 1. The solution domain is assumed unbounded in the first quadrant of the transverse plane. Carrier (ref. 1) formulated the incompressible laminar flow problem in boundary layer similarity form, and expressed the corner effects as an alteration to the Blasius solution. This analysis was incorrect however, since it failed to account for transverse plane vorticity. Rubin (ref. 2) formulated the low-speed laminar flow corner problem in completeness, using resolution of the flow domain into potential, boundary layer and corner layer regions. Subsequently, Pal and Rubin (ref. 3) and Rubin and Grossman (ref. 4) evaluated asymptotic characteristics and numerical solutions for incompressible laminar flow. Extension to laminar compressible flow is reported by Weinberg and Rubin (ref. 5). Ghia and Davis (ref. 6, 7) and Ghia (ref. 8) evaluated use of optimal coordinates for the compressible laminar flow corner. In all cited instances, numerical solutions of the governing equations were established for a symmetric half domain formed by the bisector of the right angle corner, one wall and asymptotic approach to two-dimensionality.

Tokuda (ref. 9) observed that the isovels computed by Rubin and Grossman are incorrect in comparison to the experimental data of Zamir and Young (ref. 10). This was attributed to lack of account of a fourth region tucked inside the corner layer, and he performed a Stoke's flow expansion therein and theoretically combined solutions by overlapping various regions. However, the experimental data is for turbulent flow, and Zamir and Young note a fundamental difference in the velocity contour bulges nearby the corner. As shown in Figure 2, laminar corner flow apparently induces mass entrainment directed along the walls into the corner with efflux along the bisector. For turbulent flow, the data indicates influx into the corner along the bisector with outward transport along the walls. Hence, the fundamental mechanisms for laminar and turbulent corner interaction must be distinct, and analysis of the latter is the present primary requirement.

Bragg (ref 11) analyzed turbulent incompressible corner flow and determined the distribution of Turbulence Kinetic Energy, TKE, in the corner. He observed that symmetry in a turbulent flow can occur at best only under the most controlled laboratory conditions, indicating that a full domain numerical solution is required. Eichelbrenner and Preston (ref. 12) present a comprehensive theoretical analysis of the role of secondary flow (in the transverse plane) on turbulent corner flow. They propose existence of systems of secondary vortices on the plate, see Figure 3, with the resultant corresponding pressure distribution linked to deformation in the normal components of the Reynold's stress tensor. They conclude that the resultant anisotropy of the stress is the source of the observed secondary flow behavior that induces mass flux into the corner along the bisector, see Figure 4. They further note the resultant vorticity intensity is highest if allowed to develop freely as in the unbounded juncture region. Gessner (ref. 13) refutes this analysis, presenting data which fails to indicate the required transverse pressure undulation. He presents a detailed theoretical analysis of mechanisms inducing secondary flow; an energy balance of the mean flow isolates two dominant terms responsible for observed corner influx along the bisector. Experimental data indicate that the gradient, normal to the corner bisector, of the corresponding Reynolds shear stress component, $\overline{u_l' u_n'}$, is the dominant mechanism inducing and maintaining the corner flow. The induced secondary mean flow convects axial mean velocity, vorticity and mean flow energy into the corner as a first-order effect. The axial vorticity component is a second-order effect as is the energy of the turbulence velocity field and its convection by the secondary mean flow.

The essential flow character in the juncture region thus appears the result of a delicate balance between turbulence phenomena and the induced secondary mean flow velocity field. Anisotropy of the Reynold's stress tensor is important, but apparently not a dominant influence, but the distribution of the shear components in the immediate corner region appears fundamentally important. With this insight, a parabolized form of the three-dimensional, time-averaged Navier-Stokes equations for prediction of steady, turbulent, compressible shock-free flow in a juncture region is derived. Determination of the six components of the Reynolds stress field is accomplished using a parabolic simplification to a constitutive equation. The resultant tensor field is anisotropic and requires solution of parabolized three-dimensional

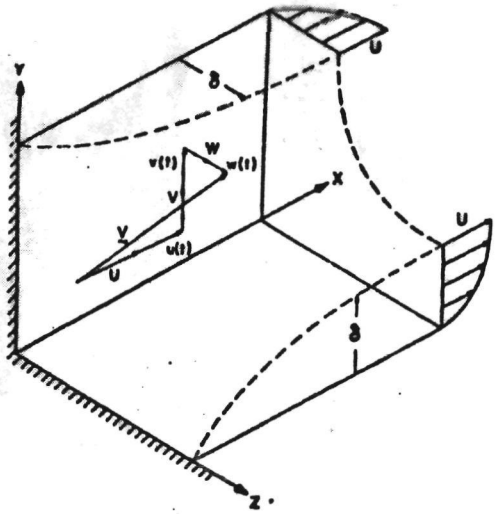

Fig. 1. Juncture Flow Geometry

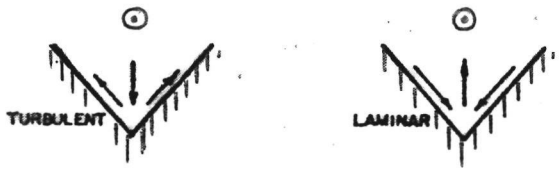

Fig. 2. Juncture Efflux/Influx

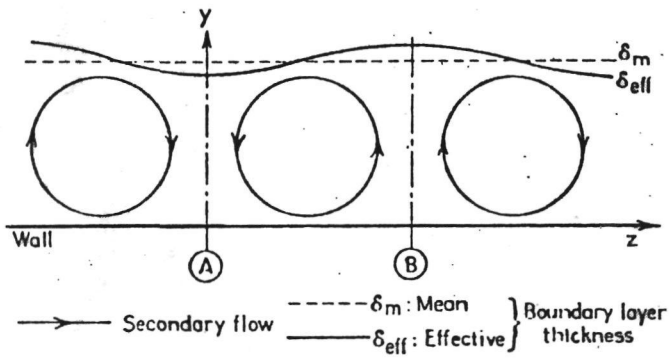

Fig. 3 Secondary Flow Structure
(Ref. 12)

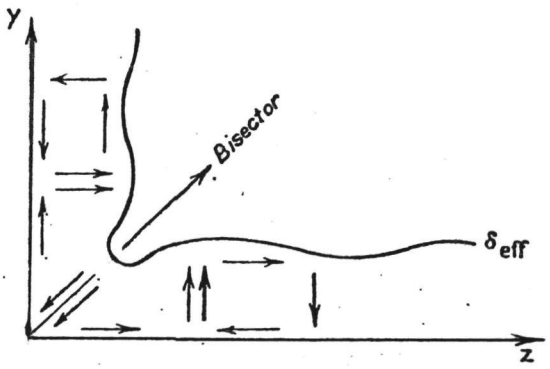

Fig. 4. Juncture Corner Influx
(Ref. 13)

forms of the transport equation for turbulence kinetic energy and isotropic dissipation function.

The developed viscous and turbulent flow description forms one part of a viscous-inviscid interaction algorithm for determination of the complete juncture region flowfield. An assumed "viscous displacement distribution" is used to generate an initial surface estimate for a three-dimensional potential flow solution. This yields the corresponding surface pressure distribution on the freestream closure segment of the viscous flow solution domain. Pressure coupling between the two solutions is accomplished through the complementary solution to a Poisson equation. The pressure particular solutions yields the detailed distribution near the juncture walls in concert with computational enforcement of conservation of mass. Following the initial solution, the computed viscous flow freestream velocities can be employed as onset velocities for a subsequent three-dimensional potential flow refinement, and an iterative interaction algorithm thereby developed.

A computer program has been written for solution of the developed three-dimensional Navier-Stokes (3DPNS) equation system. The Hess (ref. 14) computer program was employed to generate the inviscid flow pressure distribution on the juncture region surface of two intersecting non-lifting 10% thick parabolic arc airfoils with coincident leading edges and zero sweep. The 3DPNS system was solved and the three-dimensional distributions of mean velocities, Reynolds stress components, pressure distributions and onset flow refinements for the potential flow refinement determined. The results of this study are reported herein, as well as input instructions for use of the developed 3DPNS option of the COMOC III compute program for juncture region flow prediction.

SYMBOLS

a boundary condition coefficient; direction cosines

A Van Driest damping function; constant

b body force

c isentropic sound speed; coefficient

C coefficient

C_p pressure coefficient

C_p skin friction coefficient

d differential

e fintie element index

f	function of known argument; coordinate curve
Fr	Froude Number
g	gravity acceleration; function; source term
h	metric coefficient; mesh parameter; integration step size
H	boundary layer shape factor
k	thermal conductivity; turbulence kinetic energy
k	generalized diffusion coefficient
ℓ	differential operator; length scale
L	differential operator; length
M	Mach number; number of finite elements spanning R^n
n	unit normal vector; nodes per element; dimensionality
N	finite element interpolation function
p	pressure; generalized parameter; iteration index
Pr	Prandtl number
q	generalized dependent variable
Q	generalized discretized dependent variable
R	domain of elliptic operator
Re	Reynolds number
S	finite element assembly operator; surface
t	time
T	temperature
u_i	velocity vector
u,U	reference velocity
u_τ	friction velocity
v_i	computational velocity vector
x_i	Cartesian coordinate system

γ ratio of specific heats

∂R closure of solution domain R

δ Kronecker delta, boundary layer thickness; increment

δ^* boundary layer displacement thickness

Δ increment; element measure

ε turbulence dissipation function

θ boundary layer momentum thickness

η_i transformed coordinate system

ξ_i transformed coordinate system

κ Karman coefficient (MLT)

λ multiplier; turbulence sublayer constant

μ dynamic viscosity

ν kinematic viscosity; general diffusion coefficient

ρ density

σ_{ij} mean flow Stokes stress tensor

τ Reynolds stress tensor; wall shear; integration kernel

ϕ Velocity potential function

χ generalized initial-value operator

ζ_i finite element natural coordiante system

ω turbulence damping factor

Ω global solution domain

Superscripts:

e effective value

t dimension of R

t turbulent

T	matrix transpose
$+$	turbulence correlation function
$\tilde{}$	mass-weighted time-average
$\overline{\quad}$	time-averaged
$\hat{}$	unit vector
$'$	mass-weighted fluctuating component; ordinary derivative

Subscripts:

∞	global reference condition
e	finite element domain
i,j,k,ℓ	tensor indices
-	non-tensor index
I	freestream reference condition
n	normal
o	initial condition; stagnation reference
t	time derivative
w	wall reference condition

Notation:

$\{\ \}$	column matrix
$[\ ]$	square matrix
$\cup$	union
$\cap$	intersection
ε	belongs to

PROBLEM DESCRIPTION

Governing Differential Equation System

The description of a state point in multi-dimensional fluid mechanics is contained within solution of a coupled nonlinear partial differential equation system describing conservation of mass, momentum and energy. Unique solutions are obtained upon closure by specification of constitutive behavior and boundary conditions. In Cartesian tensor notation, the non-dimensional conservation form of the Navier-Stokes equation system is

$$L(\rho) \equiv \frac{\partial \rho}{\partial t} + \frac{\partial}{\partial x_j}(\rho u_j) = 0 \tag{1}$$

$$L(\rho u_i) \equiv \frac{\partial}{\partial t}(\rho u_i) + \frac{\partial}{\partial x_j}\left[\rho u_j u_i + p\delta_{ij} - Re^{-1}\sigma_{ij}\right] + Fr^{-1}\rho b_i = 0 \tag{2}$$

$$L(\rho H) \equiv \frac{\partial}{\partial t}(\rho H) + \frac{\partial}{\partial x_j}\left[\rho u_j H - (\gamma - 1)M_\infty^2 Re^{-1}\sigma_{ij}u_i - Re^{-1}Pr^{-1}\mu\frac{\partial H}{\partial x_j}\right]$$

$$- (\gamma - 1)M_\infty^2\frac{\partial p}{\partial t} = 0 \tag{3}$$

The dependent variable in equations (1)-(3) have their usual interpretation in fluid mechanics, i.e., ρ is mass density, u_j is the velocity vector, p is the static pressure, b is a body force, and H is the stagnation enthalpy. Furthermore, σ_{ij} is the Stokes stress tensor, defined as

$$\sigma_{ij} \equiv \mu\left[\frac{\partial u_j}{\partial x_j} + \frac{\partial u_j}{\partial x_i}\right] - \frac{2\mu}{3}\frac{\partial u_k}{\partial x_k}\delta_{ij} \tag{4}$$

where μ is the dynamic viscosity. The equation of state for a perfect gas closes the definition, and the non-dimensional parameters of impact are:

$$\text{Reynolds Number:} \quad Re \equiv \frac{\rho_\infty U_\infty \ell}{\mu_\infty} \tag{5}$$

$$\text{Prandtl Number:} \quad Pr \equiv \frac{c_p \mu}{k} \tag{6}$$

$$\text{Mach Number:} \quad M_\infty \equiv \frac{U_\infty}{c} \tag{7}$$

Herein, ℓ is a characteristic scale length and c is the isentropic sound speed.

Equations (1)-(7) are valid for both laminar and turbulent flows. For the latter, however, their solution becomes tractible in a practical sense only after time-averaging, and mass-weighted time-averaging is assumed to serve present requirements. Therefore, the Reynolds decomposition is defined as (ref.15)

$$u_j(x_i,t) \equiv \tilde{u}_j(x_i) + u_j''(x_i,t) \tag{8}$$

The mass-weighted time-average velocity is defined as

$$\tilde{u}_j \equiv \overline{\rho u_j}/\bar{\rho} \tag{9}$$

and

$$\overline{\rho u_i''} \equiv \lim_{T\to\infty} \int_t^{t+T} (\rho u_i - \bar{\rho}\tilde{u}_i)dt \equiv 0 \tag{10}$$

This operation yields the important relation

$$\overline{\rho u_i u_j} = \bar{\rho}\tilde{u}_i\tilde{u}_j + \overline{\rho u_i'' u_j''} \tag{11}$$

Equations (8)-(9) are also employed to define the time-averaged and fluctuating components of enthalpy as

$$\tilde{H} = \tilde{h} + \frac{1}{2}\tilde{u}_i\tilde{u}_i + \frac{1}{2}\overline{\rho u_i'' u_i''}/\bar{\rho} \tag{12}$$

Substitution of equations (8)-(9) into (1)-(4), time-averaging and collecting terms yields the time-averaged Navier-Stokes equation system

$$L(\bar{\rho}) = \frac{\partial \bar{\rho}}{\partial t} + \frac{\partial}{\partial x_j}[\tilde{u}_j\bar{\rho}] = 0 \tag{13}$$

$$L(\bar{\rho}\tilde{u}_i) = \frac{\partial(\bar{\rho}\tilde{u}_i)}{\partial t} + \frac{\partial}{\partial x_j}\left[\tilde{u}_j(\bar{\rho}\tilde{u}_i) + \bar{p}\delta_{ij} - \bar{\sigma}_{ij} + \overline{\rho u_i'' u_j''}\right] = 0 \tag{14}$$

$$L(\bar{\rho}\tilde{H}) = \frac{\partial(\bar{\rho}H)}{\partial t} + \frac{\partial}{\partial x_j}\left[\tilde{u}_j(\bar{\rho}\tilde{H}) + \overline{\rho H'' u_j''} - (\gamma - 1)M_\infty^2 Re\left(\tilde{u}_i\bar{\sigma}_{ij} + \overline{u_i''\sigma_{ij}}\right)\right.$$

$$\left. - Re^{-1}Pr^{-1}\bar{\mu}\frac{\partial \tilde{H}}{\partial x_j}\right] - (\gamma - 1)M_\infty^2\frac{\partial \bar{p}}{\partial t} = 0 \tag{15}$$

The three-dimensional parabolic Navier-Stokes (3DPNS) equations are required established to describe the steady time-averaged viscous and turbulent flow of a compressible fluid in the juncture region. The assumptions for 3DPNS are:

(1) A predominant mean flow direction is uniformly discernible.

(2) In this direction (only) diffusion processes are negligible compared to convection, and,

(3) Overall three-dimensional elliptic character is provided by interaction with the potential freestream flow.

The parabolic approximation to equations (13)-(15) basically constrains summation limits. Assuming the x_1 coordinate aligned with the direction of predominant flow, the parabolic approximation is concisely expressed as

$$\bar{\sigma}_{ij} = \frac{\bar{\mu}}{Re}(1 - \delta_{j1})\left[\frac{\partial \tilde{u}_i}{\partial x_j} + \frac{\partial \tilde{u}_j}{\partial x_i} - \frac{2}{3}\frac{\partial \tilde{u}_k}{\partial x_k}\delta_{ij}\right] \tag{16}$$

The subscript bar notation denotes the index not eligible for the summation convention, but merely takes on the value of the synonymous tensor index. The parabolic approximation to equation (15) also requires eliminating the x_1 component of ... involving the time-averaged viscosity $\bar{\mu}$. The ... dary value character on the x_1 coordinat... ields the desired form upon identification of ... model for the Reynolds stress tensor - $\overline{\rho u_i' u_j'}$.

$$\tilde{H} = \tilde{h} + \frac{1}{2}\tilde{u}_i\tilde{u}_i + \frac{1}{2}\overline{\rho u_i' u_i'}/\bar{\rho}$$

Constitutive Closure For Turbulence

The 3DPNS equation system becomes closed upon identification of the components of the Reynolds stress tensor. Based upon concepts in continuum mechanics, c.f. Lumley (ref. 16), a constitutive equation for the kinematic Reynolds stress tensor - $\overline{u_i' u_j'}$ is in the form

$$-\overline{u_i' u_j'} = -k\alpha_{ij} + C_4 \frac{k^2}{\varepsilon}\left[\frac{\partial \tilde{u}_i}{\partial x_j} + \frac{\partial \tilde{u}_j}{\partial x_i}\right] + C_2 C_4 \frac{k^3}{\varepsilon^2}\left[\frac{\partial \tilde{u}_i}{\partial x_k} + \frac{\partial \tilde{u}_k}{\partial x_i}\right]\left[\frac{\partial \tilde{u}_k}{\partial x_j} + \frac{\partial \tilde{u}_j}{\partial x_k}\right] \qquad (17)$$

The coefficients result from reexpression of triple correlations within the Reynold's stress transport equation using the model of Launder, Reece and Rodi (ref. 17). It is a generalization of the original analysis by Gessner and Emery (ref. 18) for an equilibrium steady three-dimensional parabolic flow. In equation (17) α_{ij} is a diagonal tensor defined as

$$\alpha_{ij} = \frac{1}{3k}\left(\overline{u_\ell' u_\ell'}\right) a_i \delta_{ij} \qquad (18)$$

Hence, equation (17) represents an anisotropic tensor as indicated required in the analysis of reference 12. In equation (18) the a_i are the coefficients that admit anisotropy and $a_1 \equiv C_1, a_2 = a_3 = C_3$ is suggested, where the C_i are defined by Launder, Reese and Rodi (ref. 17)as

$$C_1 \equiv \frac{22(C_{\phi 1} - 1) - 6(4C_{\phi 2} - 5)}{33(C_{\phi 1} - 2C_{\phi 2})}$$

$$C_2 \equiv \frac{4(3C_{\phi 2} - 1)}{11(C_{\phi 1} - 2C_{\phi 2})}$$

$$C_3 \equiv \frac{22(C_{\phi 1} - 1) - 12(3C_{\phi 2} - 1)}{33(C_{\phi 1} - 2C_{\phi 2})}$$

$$C_4 \equiv \frac{44C_{\phi 1} - 22C_{\phi 1}C_{\phi 2} - 128C_{\phi 2} - 36C_{\phi 2}^2 + 10}{165(C_{\phi 1} - 2C_{\phi 2})^2} \qquad (19)$$

In equations (19) $C_{\phi 1}$ and $C_{\phi 2}$ are "universal" empirical constants derived by Hanjalić and Launder (ref. 19); suggested values are $C_{\phi 1} \approx 2.8$ and $C_{\phi 2} \approx 0.45$. Additionally, in equation (17), k is the kinetic energy of the turbulence velocity field

$$\tilde{H} = \tilde{h} + \frac{1}{2}\tilde{u}_i\tilde{u}_i + \frac{1}{2}\overline{\rho u_i'' u_i''}/\bar{\rho} \qquad \overline{u_i'' u_i''} \tag{20}$$

and ε is the isotropic dissipation function defined by the contraction

$$\frac{2}{3}\delta_{ij}\varepsilon \equiv 2\bar{\nu}\,\overline{\frac{\partial u_i''}{\partial x_k}\frac{\partial u_j''}{\partial x_k}} \tag{21}$$

The governing differential equations for k and ε are (ref. 15)

$$L(k) = \frac{\partial k}{\partial t} + \frac{\partial}{\partial x_j}\left[\tilde{u}_j k - \left(C_k \frac{k}{\varepsilon}\overline{u_i'' u_j''} + \bar{\nu}\delta_{ij}\right)\frac{\partial k}{\partial x_i}\right] + \overline{u_i'' u_j''}\frac{\partial \tilde{u}_i}{\partial x_j} + \varepsilon = 0 \tag{22}$$

$$L(\varepsilon) = \frac{\partial \varepsilon}{\partial t} + \frac{\partial}{\partial x_j}\left[\tilde{u}_j\varepsilon - C_\varepsilon \frac{k}{\varepsilon}\overline{u_i'' u_j''}\frac{\partial \varepsilon}{\partial x_i}\right] + C_\varepsilon^1 \overline{u_i'' u_j''}\frac{\varepsilon}{k}\frac{\partial \tilde{u}_i}{\partial x_j} + C_\varepsilon^2 \frac{\varepsilon^2}{k} = 0 \tag{23}$$

The various C_k and C_ε^α are empirical model constants to be specified.

Three-Dimensional Parabolic Navier-Stokes Equations

The 3DPNS equation system for solution of isoenergetic juncture region flow is obtained by deletion of the time derivatives in equations (13)-(14) and (22)-(23) and eliminating the x_1 stress components in equation (17) in the manner illustrated for the Stoke's stress tensor. The resultant 3DPNS equation system requiring numerical solution is

$$\frac{\partial}{\partial x_i}(\bar{\rho}\tilde{u}_i) = 0 \tag{24}$$

$$\tilde{H} = \tilde{h} + \frac{1}{2}\tilde{u}_i\tilde{u}_i + \frac{1}{2}\overline{\rho u_i'' u_i''}/\bar{\rho}$$

$$L(\bar{\rho}\tilde{u}_1) = \frac{\partial}{\partial x_i}(\bar{\rho}\tilde{u}_i\tilde{u}_1) + \frac{\partial \bar{p}}{\partial x_1} - \frac{\partial}{\partial x_\ell}\left[\frac{\bar{\mu}}{Re}\frac{\partial \tilde{u}_1}{\partial x_\ell} - \overline{\rho u_1'' u_\ell''}\right] = 0 \tag{25}$$

$$L(\bar{\rho}\tilde{u}_2) = \frac{\partial}{\partial x_i}(\bar{\rho}\tilde{u}_i\tilde{u}_2) + \frac{\partial \bar{p}}{\partial x_2} - \frac{\partial}{\partial x_\ell}\left[\frac{\bar{\mu}}{Re}\left(\frac{\partial \tilde{u}_2}{\partial x_\ell} + \frac{\partial \tilde{u}_\ell}{\partial x_2}\right) - \overline{\rho u_2'' u_\ell''}\right] = 0 \tag{26}$$

$$L(\bar{\rho}\tilde{u}_3) = \frac{\partial}{\partial x_i}(\bar{\rho}\tilde{u}_i\tilde{u}_3) + \frac{\partial \bar{p}}{\partial x_3} - \frac{\partial}{\partial x_\ell}\left[\frac{\bar{\mu}}{Re}\left(\frac{\partial \tilde{u}_3}{\partial x_\ell} + \frac{\partial \tilde{u}_\ell}{\partial x_3}\right) - \overline{\rho u_3'' u_\ell''}\right] = 0 \tag{27}$$

$$L(k) = \frac{\partial}{\partial x_i}(\bar{\rho}\tilde{u}_i k) - \frac{\partial}{\partial x_i}\left[\bar{\rho}\left(\frac{\bar{\nu}}{Re} + C_k\frac{k}{\varepsilon}\overline{u_i'' u_k''}\right)\frac{\partial k}{\partial x_k}\right] + \overline{\rho u_i'' u_k''}\frac{\partial \tilde{u}_k}{\partial x_i} + \bar{\rho}\varepsilon = 0 \tag{28}$$

$$L(\varepsilon) = \frac{\partial}{\partial x_i}(\bar{\rho}\tilde{u}_i\varepsilon) - \frac{\partial}{\partial x_i}\left[\bar{\rho}\left(0 + C_\varepsilon\,\overline{u_i'' u_k''}\,\frac{k}{\varepsilon}\right)\frac{\partial \varepsilon}{\partial x_k}\right] + C_\varepsilon^1\,\overline{\rho u_i'' u_\ell''}\,\frac{\varepsilon}{k}\frac{\partial \tilde{u}_k}{\partial x_\ell} + C_\varepsilon^2\bar{\rho}\varepsilon^2 k^{-1} = 0 \tag{29}$$

Equations (24)-(29) introduce the 3DPNS limited summation index convention $1 \leq (i, j) \leq 3$, $2 \leq (k, \ell) \leq 3$. The dilitation term in the Stoke's stress tensor has been deleted from equations (25)-(27) as negligibly small.

The parabolic approximation to equation (17) for use in completing terms in equations (25)-(29) is (ref. 16).

$$\tilde{H} = \tilde{h} + \frac{1}{2}\tilde{u}_i\tilde{u}_i + \frac{1}{2}\overline{\rho u_i' u_i'}/\bar{\rho}$$

$$\overline{u_3' u_3'} = C_3 k - 2C_4 \frac{k^2}{\varepsilon}\frac{\partial \tilde{u}_3}{\partial x_3} \qquad - C_2 \frac{k}{\varepsilon} C_4 \frac{k^2}{\varepsilon}\left(\frac{\partial \tilde{u}_1}{\partial x_3}\right)^2$$

$$\overline{u_1' u_2'} = \qquad - C_4 \frac{k^2}{\varepsilon}\frac{\partial \tilde{u}_1}{\partial x_2}$$

$$\overline{u_1' u_3'} = \qquad - C_4 \frac{k^2}{\varepsilon}\frac{\partial \tilde{u}_1}{\partial x_3}$$

$$\overline{u_2' u_3'} = \qquad - C_4 \frac{k^2}{\varepsilon}\left[\frac{\partial \tilde{u}_2}{\partial x_3} + \frac{\partial \tilde{u}_3}{\partial x_2}\right] - C_2 \frac{k}{\varepsilon} C_4 \frac{k^2}{\varepsilon}\frac{\partial \tilde{u}_1}{\partial x_2}\frac{\partial \tilde{u}_1}{\partial x_3} \qquad (30)$$

For equation (25) the divergence term becomes

$$\frac{\partial}{\partial x_\ell}\left[\frac{\bar{\mu}}{Re}\frac{\partial \tilde{u}_1}{\partial x_\ell} - \overline{\rho u_1' u_\ell'}\right] = \frac{\partial}{\partial x_\ell}\left[\left(\frac{\bar{\mu}}{Re} + C_4\frac{\bar{\rho}k^2}{\varepsilon}\right)\frac{\partial \tilde{u}_1}{\partial x_\ell}\right]$$

Defining an "effective" kinematic viscosity

$$\nu^{eff} \equiv \frac{\bar{\nu}}{Re} + C_4\left(\frac{k}{\varepsilon}\right)k \qquad (32)$$

equation (31) becomes

$$\frac{\partial}{\partial x_\ell}\left[\frac{\bar{\mu}}{Re}\frac{\partial \tilde{u}_1}{\partial x_\ell} - \overline{\rho u_1' u_\ell'}\right] = \frac{\partial}{\partial x_\ell}\left[\bar{\rho}\nu^{eff}\frac{\partial \tilde{u}_1}{\partial x_\ell}\right] \qquad (33)$$

which corresponds exactly to the familiar boundary layer form.

In the transverse flow momentum equations (26)-(27) the divergence terms become, using equations (30)

$$\tilde{H} = \tilde{h} + \frac{1}{2}\tilde{u}_i\tilde{u}_i + \frac{1}{2}\overline{\rho u_i' u_i'}/\bar{\rho} = \frac{\partial}{\partial x_\ell}\left[\bar{\rho}\nu_{eff}\left(\frac{\partial \tilde{u}_k}{\partial x_\ell} + \frac{\partial \tilde{u}_\ell}{\partial x_k}\right)\right]$$

$$- \frac{\partial}{\partial x_\ell}\left[\bar{\rho}k\alpha_{k\ell} - \bar{\rho}C_2\frac{k}{\varepsilon}C_4\frac{k}{\varepsilon}k\frac{\partial \tilde{u}_1}{\partial x_k}\frac{\partial \tilde{u}_1}{\partial x_\ell}\right] \qquad (34)$$

The first right-hand term is basically identical to equation (33) for $\tilde{u}_1$, with the addition of terms involving shear of the alternative transverse plane mean velocity component $\tilde{u}_\ell$. The second term is a non-homogeneity involving only shear components of the predominant velocity $\tilde{u}_1$ which acts as a source term within the transverse momentum equations.

The divergence term common to both the k and ε equations becomes

$$\frac{\partial}{\partial x_i}\left[\frac{1}{3}C_q\bar{\rho}\frac{k}{\varepsilon}\overline{u_i' u_\ell'}\frac{\partial q}{\partial x_\ell}\right] = \frac{\partial}{\partial x_\ell}\left[\frac{2}{3}C_q\bar{\rho}\frac{k^2}{\varepsilon}\frac{\partial q}{\partial x_\ell}\right] \qquad (35)$$

where q represents either k or ε. Equation (35) is identical to the Reynold's stress contribution in equation (32) with C_4 replaced by C_q. The production terms for both k and ε are basically identical, with the latter multiplied by $C_\varepsilon^1 \varepsilon/k$. The Reynold's stress-velocity shear contraction under the parabolic approximation becomes

$$\overline{\rho u_i' u_k'}\frac{\partial \tilde{u}_i}{\partial x_k} = \bar{\rho}C_4\frac{k^2}{\varepsilon}\left[\frac{\partial \tilde{u}_1}{\partial x_\ell}\frac{\partial \tilde{u}_1}{\partial x_\ell}\right] + 2\bar{\rho}C_2\frac{k}{\varepsilon}C_4\frac{k}{\varepsilon}k\left(\frac{\partial \tilde{u}_1}{\partial x_1}\right)\left[\frac{\partial \tilde{u}_1}{\partial x_\ell}\frac{\partial \tilde{u}_1}{\partial x_\ell}\right] \qquad (36)$$

The second term is assumed negligible due to the appearance of $\partial\tilde{u}_1/\partial x_1 << \partial\tilde{u}_1/\partial x_\ell$.

Pressure Resolution and Mass Conservation

A key element for the viscous-inviscid interaction algorithm for juncture region flow is the pressure coupling between the two flowfield descriptions. Solution of the full three-dimensional linear Laplacian equation governing the inviscid, assumed-irrotational subsonic exterior flow can be readily accomplished with current computer programs, e.g., ref. 14. This is possible using the computational equivalent of either flow tangency boundary conditions (on a stream surface) or specification of the "onset" velocity on any surface.

This is defined as the difference between the local velocity vector and reference freestream vector. Many two-dimensional interaction algorithms assume that the (aerodynamic) surface augmented by the boundary layer displacement thickness δ^* corresponds to the inviscid streamline. However, since δ^* could be difficult to define for other than an elementary juncture geometry, the specifications and iterative refinement of the inviscid onset velocity appears more attractive.

This is the sole boundary condition requirement for determination of the three-dimensional inviscid flow pressure distribution (C_p) on the viscous flow domain intersection with the freestream. The point of departure for derivation of the pressure coupling algorithm is the steady parabolized form mean flow momentum equations,(25)-(27). It is based on the two-dimensional transverse plane Poisson equation obtained by application of the divergence operator. Recalling the limited summation convention, $1 \leq j \leq 3$, and $2 \leq k, \ell \leq 3$, this equation takes the form

$$L(\bar{p}) = \frac{\partial}{\partial x_\ell}\left[\frac{\partial \bar{p}}{\partial x_\ell} + \frac{\partial}{\partial x_j}\left(\bar{\rho}\tilde{u}_j\tilde{u}_\ell\right) - \frac{\partial}{\partial x_k}\left(\bar{\sigma}_{\ell k} - \overline{\rho u''_\ell u''_k}\right)\right] = 0 \qquad (37)$$

The algorithm is based upon the observation that the solution of a linear, elliptic Poisson equation consists of a complementary and a particular contribution as

$$\bar{p}(x_i) = p_c(x_i) + p_p(x_i) \qquad (38)$$

By definition, the complementary solution satisfies the homogeneous part of equation (37), i.e.,

$$L(p_c) = \frac{\partial^2 p_c}{\partial x_\ell^2} = 0 \qquad (39)$$

subject to the known boundary conditions for $\bar{p}(x_i)$. Since the bounding inviscid flow pressure distribution is everywhere known,

$$\bar{p}(\bar{x}_\ell) = p^I(\bar{x}_\ell) = p_c(\bar{x}_\ell) \qquad (40)$$

In equation (40), $\bar{x}_\ell$ indicates x_ℓ constrained to the boundary of the viscous solution domain, $\partial\Omega = \partial R^2 \times x_1$, and p^I is the (inviscid flow) pressure level distribution. Elsewhere on $\partial\Omega$, the appropriate boundary condition is vanishing normal gradient, i.e.,

$$\ell(p_c) = \frac{\partial}{\partial x_\ell} p_c \cdot \hat{n}_\ell = 0 \qquad (41)$$

The particular solution p_p is any function satisfying equation (37) with homogeneous boundary conditions on closure segments of Ω coincident with pI known. Elsewhere, the boundary condition for p_p is established from the inner product of the parent steady momentum equations (26)-(27) with the closure surface normal. Since the convection term vanishes identically at a wall or symmetry plane, the appropriate form is

$$\ell(p_p) = \frac{\partial p}{\partial x_\ell}\hat{n}_\ell - \frac{\partial}{\partial x_k}\left[\bar{\sigma}_{\ell k} - \overline{\rho u_k' u_\ell'}\right]\hat{n}_\ell = 0 \qquad (42)$$

Furthermore, since retaining the second term in equation (42) obliterates the appearance of the boundary condition stress term in equation (37), the appropriate Poisson equation for p_p must be the inviscid form, i.e.,

$$L(p_p) = \frac{\partial}{\partial x_\ell}\left[\frac{\partial p_p}{\partial x_\ell} + \frac{\partial}{\partial x_j}\bar{\rho}\tilde{u}_j\tilde{u}_\ell + \frac{\partial}{\partial x_k}\overline{\rho u_\ell' u_k'}\right] = 0 \qquad (43)$$

Equations (37)-(43) define the algorithm for determination of the pressure distributions within the three-dimensional parabolic viscous flow solution domain. The overall elliptic character of the subsonic flowfield is enforced by the fully three-dimensional exterior potential flow pressure distribution boundary conditions. Hence, a sequential iteration between the two problem specifications is required. To avoid a possible destabilizing of the parabolic equation solution, the axial pressure gradient distributions driving $\tilde{u}_1$ are assumed constituted solely of the complementary pressure field. The current computed particular and complementary pressures are summed to form the gradients in the plane transverse to $\tilde{u}_1$. Following the first sweep of the parabolic solution, a refined complementary field is constructed from the three-dimensional potential flow solution on the modified viscous surface. For the second parabolic solution, the current complementary and previous-iterate particular pressure distribution are added to form the axial pressure gradient for $\tilde{u}_1$. Hence, in convergence of the interaction algorithm, the current-iterate particular pressure distribution should become negligibly small.

Equation (43) can be simplified by insertion of the continuity equation (24). However, a direct enforcement of conservation of mass is also required established. Hence, assume the solution mean flow velocity field $\tilde{u}_i$ comprised of the sum of the solution $\tilde{v}_i$, of the steady flow momentum equations (25)-(27), and an irrotational correction velocity field determined from a potential distribution ϕ as (ref. 20, 21)

(44)

The steady velocity field $\tilde{u}_i$ must satisfy the continuity equation (24); hence, substituting equation (44) yields

$$L(\phi) = \frac{\partial}{\partial x_\ell}\left(\bar{\rho}\frac{\partial \phi}{\partial x_\ell}\right) - \frac{\partial}{\partial x_i}(\bar{\rho}\tilde{v}_i) = 0 \qquad (45)$$

Therefore, the correction velocity field satisfies a Poisson equation that becomes homogeneous in the limit as $\bar{\rho}\tilde{v}_i$ becomes divergence-free, i.e., equal to $\bar{\rho}\tilde{u}_i$. The boundary condition for solution of equation (45) is expressed in the inner product of equation (44) with the outward pointing normal to the solution domain closure $\partial\Omega$. Since $\tilde{v}_i$ is required to satisfy the boundary conditions for $\tilde{u}_i$, this yields

$$\ell(\phi) = \frac{\partial \phi}{\partial x_\ell}\hat{n}_\ell = 0 \qquad (46)$$

Therefore, equations (45)-(46) define the Newmann problem; ϕ must be set to a constant at least at one nodal location on $\partial\Omega$ to render the solution unique.

Since the differential specifications for particular pressure and perturbation velocity are elliptic, their solutions are obtainable upon convergence of the parabolic equation solutions at any (each) axial station. A dominant term in the non-homogeniety of equation (45) occurs for i = 1, which corresponds to the axial derivation of the $\tilde{u}_1$ velocity component. This is evaluated at the current x_1 station using a second-order accurate backwards difference formula. Upon determination of the distribution of ϕ, the particular pressure equation is solvable since the divergence-free field $\bar{\rho}\tilde{u}_i$ is known. At this point all dependent variable distributions are known at the current station. Based upon the previous station data, distributions for all variables at the next x_1 station are predicted using a second-order accurate difference formula. The predicted values of parabolic variables are corrected by solving the initial-valued differential equations. Following convergence, the remaining variables are then corrected by solution of the elliptic differential equations.

Coordinate Transformation For Juncture Region Geometry

At this point in the development, the juncture region is assumed formed by two non-lifting intersecting surfaces with coincident leading edges, denoted S_1 and S_2 in Figure 5. The viscous juncture flow boundary-value solution domain R^2 is bounded by the envelope of S_1 and S_2, denoted $f_{\ell 1}(x_1)$, the viscous intersection with the inviscid freestream, denoted $f_{\ell 2}(x_1)$, and two straight lines connecting their extremities, as noted in Figure 5. The surfaces S_1 and S_2 are not coordinate surfaces of x_i; however, the $f_{\ell i}$ are simply displacements parallel to the appropriate coordinate x_ℓ. For R^2, the transformation $\eta_i = \eta_i\,(x_i, f_{\ell i})$ that normalizes coordinates is

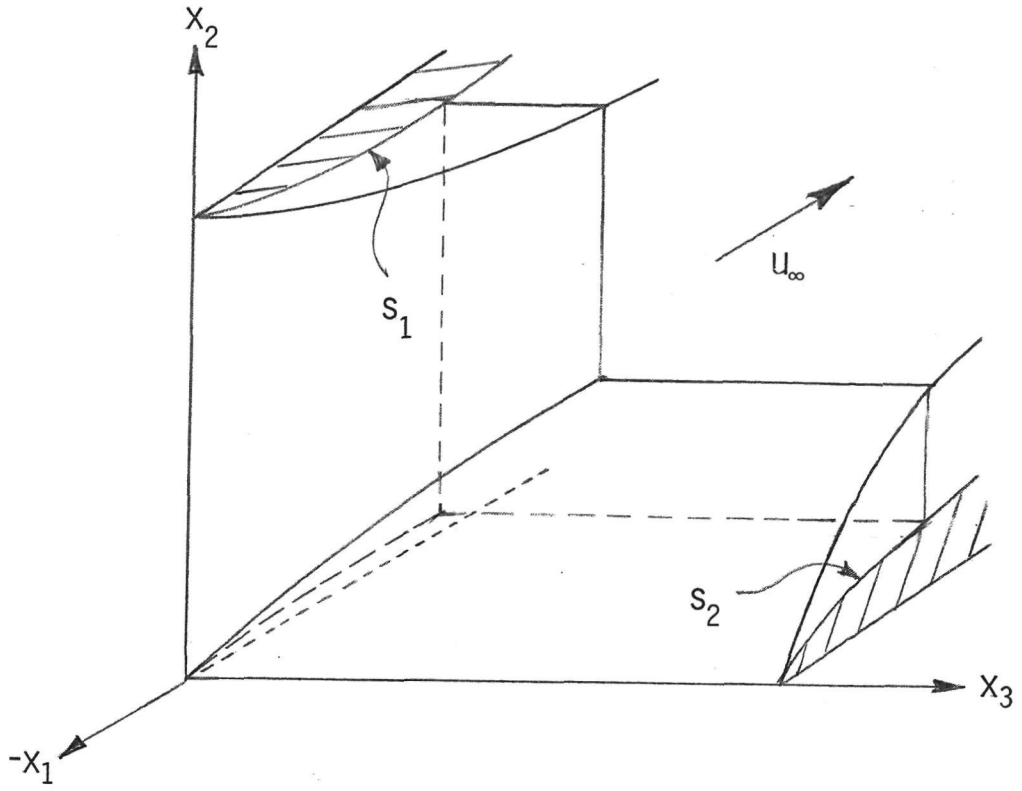

Figure 5. Juncture Corner Formed By Intersecting Parabolic Arcs

$$\{\eta_i\} \equiv \left\{ \begin{array}{c} x_1 \\ \dfrac{x_2 - f_{21}(x_1)}{[f_{22}(x_1) - f_{21}(x_1)]/f_2} \\ \dfrac{x_3 - f_{31}(x_1)}{[f_{32}(x_1) - f_{31}(x_1)]/f_3} \end{array} \right\} \tag{47}$$

Here, the $f_{\ell i}(x_1)$ are assumed (at least) piecewise continuous curves describing the closure and f_ℓ are normalizing coefficients. For example, shown in Figure 6 is a two-dimensional representation, where f_{21} is piecewise continuous while f_{22} is smooth. Using the chain rule, differentiation on x_1 introduces additional differential terms on η_ℓ. In particular,

$$\frac{\partial}{\partial x_1} = \frac{\partial}{\partial \eta_1} - \left[h_{22} + \eta_2 h_{23}\right]\frac{\partial}{\partial \eta_2} - \left[h_{32} + \eta_3 h_{33}\right]\frac{\partial}{\partial \eta_3}$$

$$\frac{\partial}{\partial x_2} = h_{21}\frac{\partial}{\partial \eta_2} \tag{48}$$

$$\frac{\partial}{\partial x_3} = h_{31}\frac{\partial}{\partial \eta_3}$$

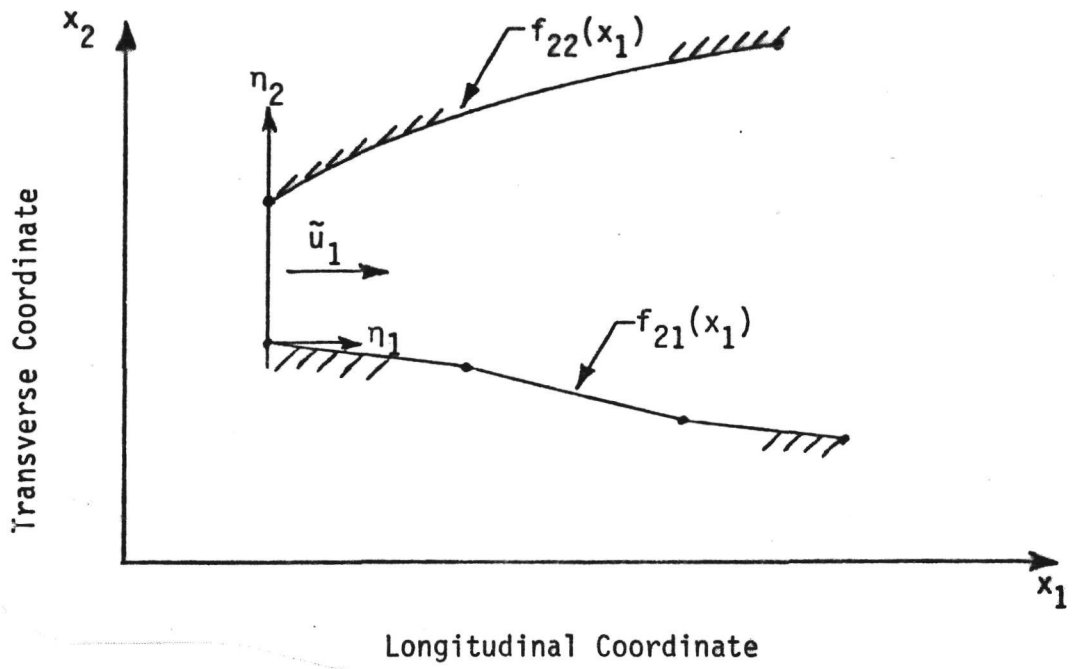

Figure 6. Coordinate System Transformation

The functions $h_{\ell i}$, $1 \leq i \leq 3$, are related to the metric of the coordinate transformation, equation (47), and are defined as

$$\{h_{\ell i}\} \equiv \begin{Bmatrix} f_\ell (f_{\ell 2} - f_{\ell 1})^{-1} \\ h_{\ell 1} f'_{\ell 1} \\ h_{\ell 1} f_\ell^{-1} (f'_{\ell 2} - f'_{\ell 1}) \end{Bmatrix} \tag{49}$$

The superscript prime denotes the ordinary derivative with respect to x_1. The η_i coordinate system is fixed in the transform space and hence insensitive to x_1. This non-orthogonal coordinate transformation is generally valid for 3DPNS solutions provided the mean flow velocity vector $\tilde{u}_i$ remains essentially parallel to η_1. A curvilinear orthogonal transformation would be required to describe flows over highly curved surfaces using 3DPNS.

Boundary Condition Specifications

Figure 7 illustrates the viscous flow solution domain closure on the x_ℓ plane. Pressure coupling with the three-dimensional inviscid exterior flow is accomplished by equating the complementary pressure p_C to p^I on closure segment d-e-f. Furthermore, $p_C \equiv p^I$ on segments c-d and f-a since these are assumed sufficiently remote such that boundary layer flow

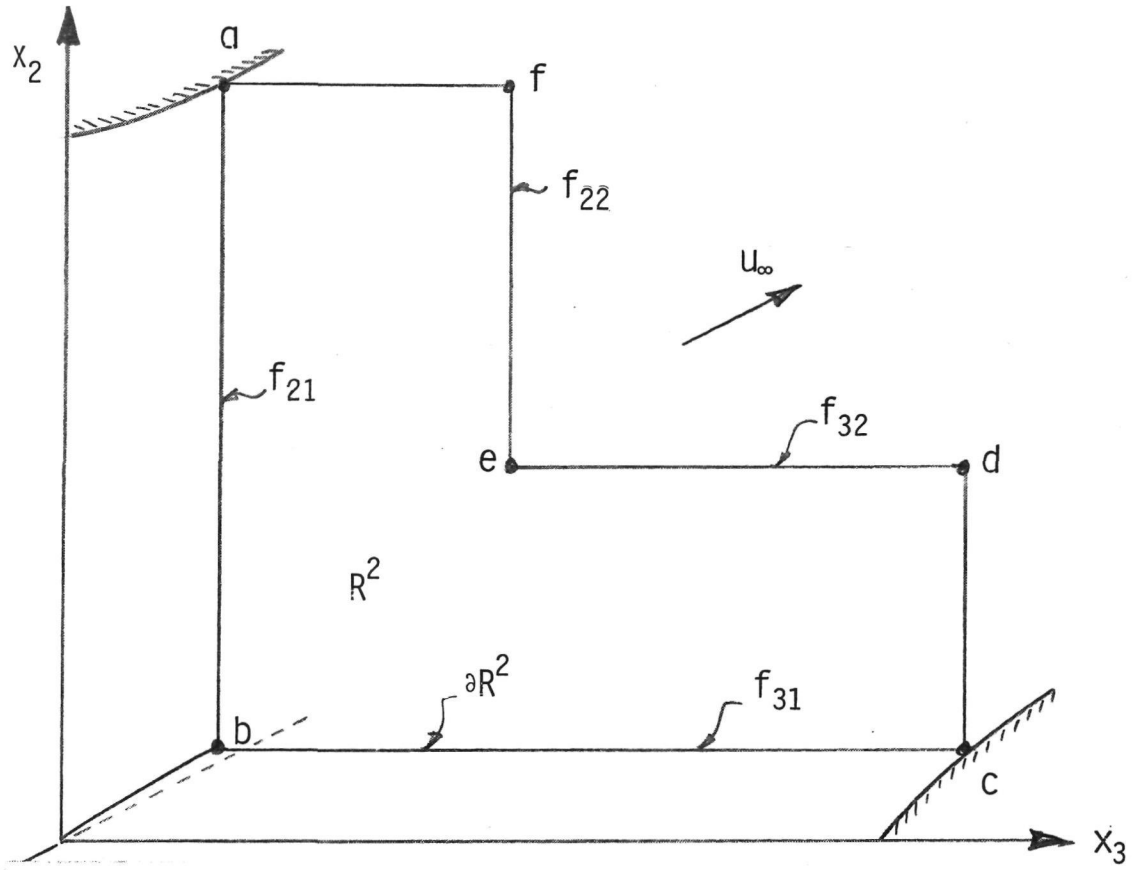

Figure 7. Juncture Region 3DPNS Boundary Conditions

exists thereupon. The normal derivative of p_c vanishes on segment a-b-c. The particular pressure p_p is zero on segment c-d-e-f-a, and its normal derivative is constrained according to equation (42) on a-b-c.

No-slip boundary conditions are applied on the juncture region surface, $f_{\ell 1}$, hence segment a-b-c in Figure 7. The x_3-derivative of both $\tilde{u}_1$ and $\tilde{v}_3$ are assumed to vanish on c-d, and $\tilde{u}_2$ can be solved directly from the primitive form of the continuity equation (24) as

$$\frac{\partial(\bar{\rho}\tilde{v}_2)}{\partial x_2} = - \frac{\partial(\bar{\rho}\tilde{u}_1)}{\partial x_1} \tag{50}$$

Similarly on segment f-a, the x_2-derivative of $\tilde{u}_1$ and $\tilde{v}_2$ vanishes and

$$\frac{\partial(\bar{\rho}\tilde{v}_3)}{\partial x_3} = - \frac{\partial(\bar{\rho}\tilde{u}_1)}{\partial x_1} \tag{51}$$

Note the right-hand side of both equations (50)-(51) contains the axial derivative of $\bar{\rho}\tilde{u}_1$, which is formed using a second-order accurate backwards difference formula. The continuity equation and the irrotational constraint

for the inviscid exterior flow are used to derive gradient constraint boundary conditions for $\tilde{v}_\ell$ on the freestream closure segment. On e-f, this yields

$$\frac{\partial \tilde{v}_2}{\partial x_3} = \frac{\partial \tilde{v}_3}{\partial x_2} \tag{52}$$

$$\frac{\partial(\bar{\rho}\tilde{v}_3)}{\partial x_3} = - \frac{\partial(\bar{\rho}\tilde{u}_1)}{\partial x_1} - \frac{\partial(\bar{\rho}\tilde{v}_2)}{\partial x_2} \tag{53}$$

On segment d-e the 2 and 3 subscripts in equations (52)-(53) are permitted. The normal derivative of the perturbation velocity potential function ϕ must vanish everywhere on ∂R^2, as described previously except for being set to zero at one location.

The boundary conditions for turbulence kinetic energy and dissipation function are vanishing normal derivative on segemtns c-d and f-a, and identical vanishing on the freestream segment d-e-f and the wall a-b-c. An adequate resolution of the transitional sublayer appears computationally uneconomical in terms of required discretization. Therefore, mixing length theory and definition of a dissipation length scale are employed to establish k and ε at computational nodes lying closer to the wall than a specified level of the turbulence Reynolds number y+,

$$y+ \equiv \frac{\bar{\rho} u_\tau x_n}{\bar{\mu}} \tag{54}$$

In equation (54), x_n is the coordinate x_ℓ perpendicular to the wall, and u_τ is the friction velocity

$$u_\tau \equiv \left[\frac{\tau_w}{\bar{\rho}}\right]^{\frac{1}{2}} \tag{55}$$

where τ_w is the $\tilde{u}_1$ wall shear stress. In the near wall region, mixing length theory (ref. 15) yields the alternative expression for ν^{eff}.

$$\nu^{eff} = \frac{\bar{\nu}}{Re} + \omega^2 \ell^2 \left[\frac{\partial u_1}{\partial x_n}\right] \tag{56}$$

where ω is Van Driest wall damping and ℓ is the mixing length. Comparing equations (56) and (32) yields, for $x_n \leq y+$

$$C_4 \frac{k^2}{\varepsilon} \approx \omega^2 \ell^2 \left| \frac{\partial \tilde{u}_1}{\partial x_n} \right| \tag{57}$$

The additional required relation is definition of the dissipation length scale ℓ_d

$$\ell_d \equiv C_\nu \frac{k^{3/2}}{\varepsilon} \tag{58}$$

which, for $x_n \leq y^+$ is assumed of the form

$$\ell_d = C_\nu^{1/4} \kappa x_n \tag{59}$$

In equation (59), κ is the von Karman constant (0.435).

Finite Element Solution Algorithm

The 3DPNS partial differential equation system for the viscous juncture region flow is identified. Each member of the equation set (25)-(29), (39), (43) and (45) belongs to the general class of second-order non-linear elliptic partial differential equations. Hence, for $\{q\} \equiv \{\tilde{u}_1, \tilde{v}_\ell, k, \varepsilon, p_c, p_p, \phi\}$ each equation is of the form,

$$L(q) = \frac{\partial}{\partial x_\ell}\left[K \frac{\partial q}{\partial x_\ell}\right] + f_1\left(q, \frac{\partial q}{\partial x_\ell}, p, x_i\right) + f_2\left(\tilde{u}_1, \frac{\partial q}{\partial x_1}\right) = 0 \tag{60}$$

In equation (60), the tensor indices range $2 \leq \ell \leq 3$, and $1 \leq i \leq 3$, K is the diffusion coefficient, f_1 is a function of its argument that specifically includes three-dimensional convection, p is any solution parameter including another dependent variable, and f_2 is the initial-value operator if present. The three-dimensional solution is required established on the bounded open domain Ω

$$\Omega \equiv R^2 x \left[\chi_0, \chi\right) \varepsilon \, x_\ell \times \left[x_1(0), x_1\right) \tag{61}$$

Note in equations (39), (43) and (45) f_2 vanishes identically and x_1 appears only as a parameter. The general functional constraint for all q on the closure $\partial\Omega$ of Ω, i.e., $\partial\Omega \equiv \partial R^2 x \left[\chi_0, \chi\right) \varepsilon \, \bar{x}_\ell \times x_1$ is

$$\ell(q) = a_1\, q + a_2\, K\frac{\partial q}{\partial x_\ell}\, n_\ell + a_3 = 0 \tag{62}$$

where the $a_i(\bar{x}_\ell, x_1)$ are specified. Except for $q = \{p_c, p_p, \phi\}$, an initial condition is required on $R^2 \cup \partial R^2 \times x_1\,(0)$ as

$$q(x_1(0), x_2, x_3) \equiv q_0(x_2, x_3) \tag{63}$$

The finite element algorithm assumes all q and p interpolated on Ω as

$$q_e(x_\ell, x) = \{N_k(x_\ell)\}^T \{Q(x)\}_e \tag{64}$$

Determination of the expansion coefficients is accomplished using the Method of Weighted Residuals (ref. 22) as

$$S_e\left[\int_{R_e^2} \{N(x_\ell)\}\, L(q_e)\, d\tau - \lambda \int_{R_e^2 \cap \partial R^2} \{N(x_\ell)\}\, \ell(q_e)\, d\tau\right] \equiv \{0\} \tag{65}$$

where S_e is the assembly operator. The assembled finite element algorithm for the representative partial differential equation system is then

$$S_e\left[-\int_{R_e^2} \frac{\partial}{\partial x_\ell}\{N\}\, K\frac{\partial q_e}{\partial x_\ell}\, d\tau + \int_{R_e^2} \{N\}\,(f_{1e} + f_{2e})\, d\tau - \int_{\partial R_e^2 \cap \partial R} \{N\}\left[a_1\, q_e + a_3\right] d\tau\right] \equiv \{0\} \tag{66}$$

The rank of the global equation (66) is identical with the total number of node points on $R^2 \cup \partial R^2$ at which the dependent variable requires solution. For f_2 non-vanishing, equation (66) is a system of first-order ordinary differential equations. For f_2 vanishing identically, it is large order algebraic, and the matrix structure is symmetric, sparse and banded.

An implicit solution algorithm is employed to solve equation (66) for all initial-value problem descriptions. The explicit form for equation (66) is

$$S_e \left[[C]_e \{q\}'_e + ([U]_e + [K]_e)\{Q\}_e + \{f\}_e \right] \equiv \{0\} \tag{67}$$

The superscript prime denotes the ordinary derivative with respect to the x_1 (η_1) coordinate. The matrix expressions for the first three terms, which account for axial convection and transverse plane convection and diffusion respectively, are

$$\begin{aligned}
[C]_e &\equiv \{\bar{\rho}\tilde{u}_1\}_e^T \int_{R_e^2} \{N\}\{N\}\{N\}^T d\tau \\
[U]_e &\equiv \{\bar{\rho}\tilde{u}_\ell\}_e^T \int_{R_e^2} \{N\}\{N\}\frac{\partial\{N\}}{\partial x_\ell} d\tau \\
[K]_e &\equiv \{\bar{\rho}\nu^{eff}\}_e^T \int_{R_e^2} \{N\}\frac{\partial\{N\}}{\partial x_\ell}\frac{\partial\{N\}}{\partial x_\ell} d\tau
\end{aligned} \tag{68}$$

Summation on $2 \leq \ell \leq 3$ is implied, and derivatives on x_i are replaced by equations (48) in the sequel. All terms not explicitly involving q, i.e., $\{Q\}$, are contained in $\{f\}_e$.

The single-step implicit integration algorithm employed is

$$\{Q\}_{j+1} = \{Q\}_j + h\left[\theta\{Q\}'_{j+1} + (1 - \theta)\{Q\}'_j\right] \tag{69}$$

In equation (69), j is the axial station index, h is integration step-size, and θ equals one-half yields the trapezoidal rule. Following the usual matrix manipulations, insertion of equation (67) into (69) yields a large order, non-linear algebraic equation system. The Newton matrix iterative algorithm for solution of this system is employed as

$$\left[J\left(\{Q\}_{j-\ell}\right)\right]\{\delta Q\}_{j+1}^{p+1} = -\left\{F\left(\{Q\}_{j+1}^{p}\right)\right\} \tag{70}$$

The dependent variable in equation (70) is the iteration vector, and

$$\{Q\}_{j+1}^{p+1} \equiv \{Q\}_{j+1}^{p} + \{\delta Q\}_{j+1}^{p+1} \tag{71}$$

where p is the iteration index, and $\ell > 0$ is an integer that retards evaluation of the Jacobian as an economy measure. The right side of equation (70) is the homogeneous form of equation (69) evaluated with the $p^{\underline{th}}$ iterate, i.e.,

$$\{F\}_{j+1}^{p} = S_e\left[[C]_e\left(\{Q\}_{j+1}^{p} - \{Q\}_j\right) + h\left(\theta\{g_e\}_{j+1}^{p} + (1-\theta)\{g_e\}_j\right)\right] \tag{72}$$

where

$$\{g_e\}_{\ell}^{p} \equiv \left([U]_e + [K]_e\right)\{Q\}_{\ell}^{p} + \{f\}_e \tag{73}$$

Equations (72)-(73) are defined only in terms of inner products on elements, with the assembly operator yielding the equivalent global expression. The vanishing of {F}, to within definition of a computed zero, yields equation (70) homogeneous, hence convergence of the iteration for any evaluation of the Jacobian. The initial estimate $\{Q\}_{J+1}^{1}$ for any iteration can be determined using $\theta = 0$.

By definition, the Jacobian [J] for equation (70) is the derivative of equation (72) with respect to $\{Q\}_{j+1}^{p}$. Each of the finite element matrices $[C]_e$, $[U]_e$ and $[K]_e$ have imbedded therein functional dependence on each $\{Q\}_{j+1}^{p}$, see equations (68), and an exact evaluation of [J] is difficult. However, the exact Jacobian is not required by the formulation; an economical approximation useful for all five dependent variables is (ref. 23).

$$[J] \equiv S_e\left[[C]_e + h\theta\left([U]_e + [K]_e\right)\right] \tag{74}$$

The $[C]_e$ and $[U]_e$ element matrices contain the exact non-linearity due to convection, while $[K]_e$ accounts for the essential diffusive non-linearity as approximated by the effective viscosity. Dependent upon the overall behavior of the solution of equation (70), equation (74) can be updated every iteration with $\{Q\}^p_{j+1}$, evaluated once every step with $\{Q\}_j$, the previous converged iterate, or maintained at the evaluation of any converged iterate, $\{Q\}_{j-\ell}$. In any case, the operations in equation (74) are limited to matrix inner products on an elemental basis. The rank of $[J]$ equals the order of $\{\delta Q\}$; specific (Dirichlet) boundary constraints are applied within the evaluation of $\{F\}$.

NUMERICAL RESULTS

Solution Initiation

The basic requirement is to assess accuracy and stability of the developed code for the 3DPNS solution algorithm. The test case corresponds to onset flow at zero angle of attack into a right juncture corner formed by coincident leading edge surfaces. The viscous displacement surface for the exterior three-dimensional potential flow is assumed the right intersection of two 10% thick parabolic arcs. The Hess computer program (ref. 14) was executed at NASA Langley using a (fine) discretization containing approximately 5000 surface panels to produce the inviscid pressure distribution. Figure 8 shows computed spanwise distribution of potential C_p at three chord stations. The influence of the corner at the first two stations extends about 0.3 y/C spanwise. The 3DPNS evaluation was conducted using the inviscid C_p distributions within the interval $0.04 < x_1/C < 0.14$, wherein influence of the corner juncture was dominant within the first quarter chord.

Figure 9 illustrates a representative 3DPNS corner discretization of R^2, plotted without diagonals. The first step in the solution is to determine a sufficient number of complementary pressure distributions, since these depend only upon $C_p(\bar{x}_\ell\ ,\ x_1)$, see equations (39)-(40). Core storage is minimized by solving only three distributions of $p_c(x_\ell,\ x_1^1)$ and interpolating to evaluate both $p_c(x_\ell)$ and the axial pressure gradient $\partial p_c/\partial x_1$ distributions at x_1 stations of the 3DPNS solution. Figures 10 and 11 illustrate the computed (dynamic) p_c and x_1-derivative of p_c distributions at the initial station for the test case. Each row of data corresponds to the nodal distribution on "columns," extending from the wall to freestream, starting at the top-left extremity of Figure 9.

The 3DPNS solution is initialized at a selected $x_1(0)$ by using Cole's law (ref. 15) to imbed a turbulent $\tilde{u}_1$ velocity profile on each node "column" with freestream value matched to the inviscid C_p. Figure 12 illustrates the initial $\tilde{u}_1$ so obtained for the test case. Initial distributions for k and ε are self-generated by the program using the initial $\tilde{u}_1$ distribution, by extending onto R^2 the mixing length concepts employed for the transition layer model. The sole requirement is to expand the dissipation length scale definition, equation (59) to the local boundary layer thickness δ. This is accomplished in the program using an exponential decay term such that $\ell_d(\delta) = C_\nu \delta$. Then, equations (58)-(59) are combined with equation (57) to yield a solution for k and ε. The initial distributions of k and ε for the test case are shown in Figures 13-14.

The transverse velocity field $\tilde{v}_\ell$, plus the ϕ and p_p solutions, cannot be evaluated at the initial solution plane, since each requires evaluation of $\partial\tilde{u}_1/\partial x_1$. Therefore, $\tilde{u}_\ell$ and p_p must be assumed initially zero.

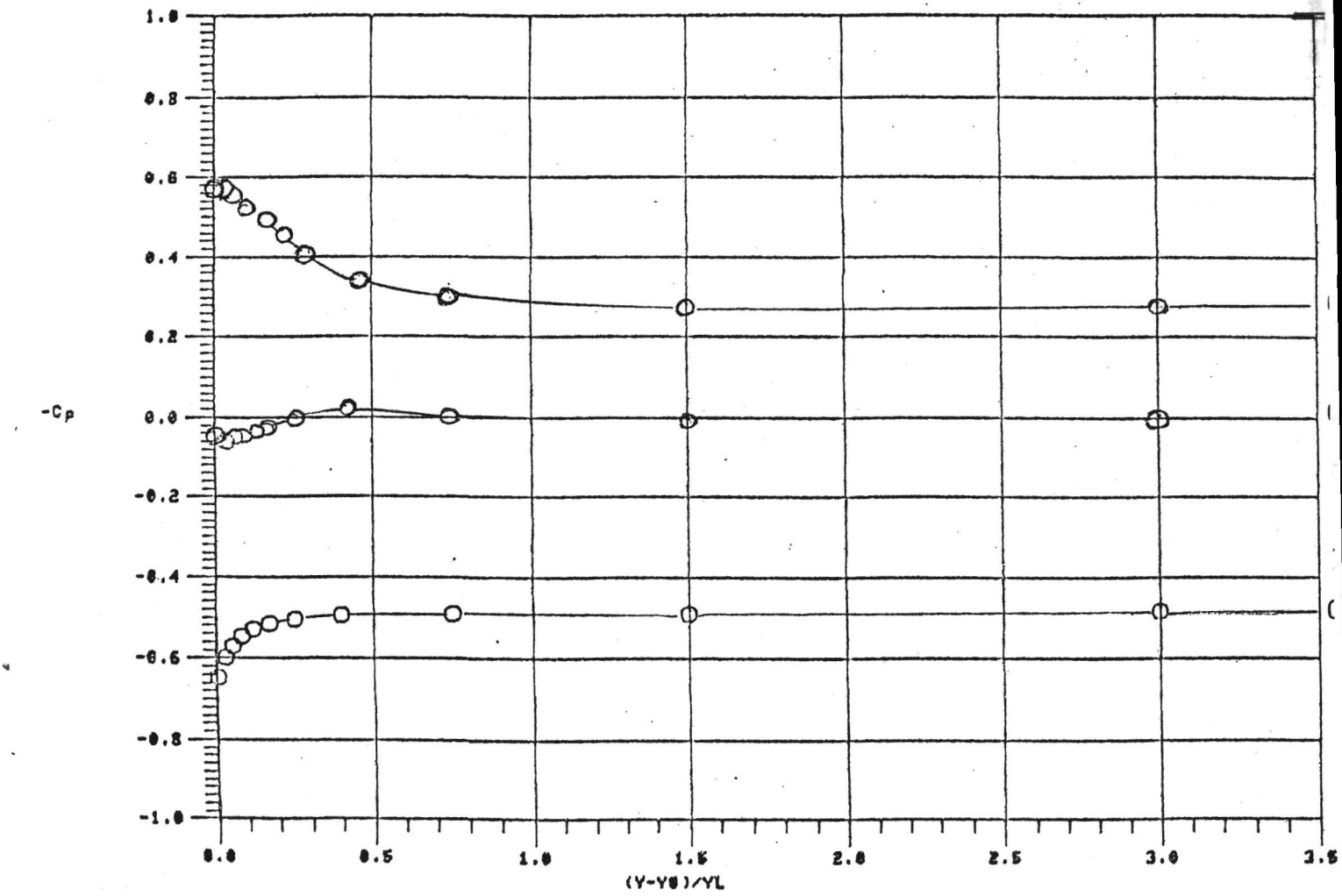

Figure 8. Computed Juncture Region Potential Flow Pressure Distributions For 10% Thick Parabolic Arc Intersection

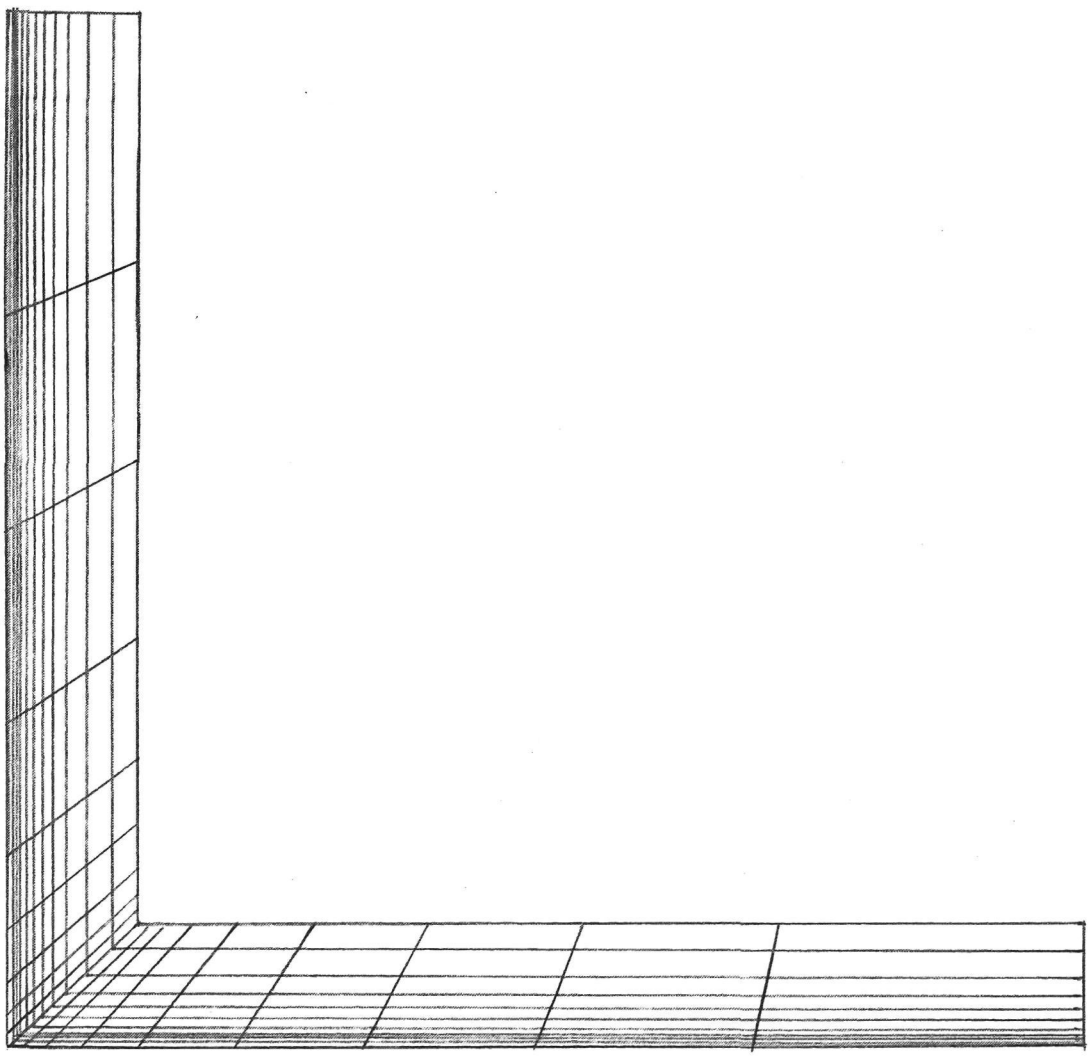

Figure 9. Finite Element Discretization Of 3DPNS Solution Domain

	PCD / PREF E 0									
1	-0.437687	-0.437687	-0.437687	-0.437687	-0.437687	-0.437687	-0.437687	-0.437687	-0.437687	-0.437687
2	-0.430000	-0.430000	-0.430027	-0.430065	-0.430120	-0.430199	-0.430315	-0.430488	-0.430752	-0.431161
3	-0.421550	-0.421550	-0.421612	-0.421700	-0.421826	-0.422004	-0.422261	-0.422633	-0.423180	-0.423998
4	-0.412880	-0.412880	-0.412982	-0.413125	-0.413327	-0.413612	-0.414019	-0.414602	-0.415448	-0.416693
5	-0.404870	-0.404870	-0.405000	-0.405183	-0.405439	-0.405799	-0.406307	-0.407033	-0.408096	-0.409706
6	-0.398716	-0.398716	-0.398839	-0.399010	-0.399246	-0.399572	-0.400024	-0.400659	-0.401586	-0.403048
7	-0.395276	-0.395276	-0.395357	-0.395468	-0.395617	-0.395816	-0.396080	-0.396426	-0.396889	-0.397582
8	-0.394036	-0.394036	-0.394069	-0.394116	-0.394177	-0.394255	-0.394348	-0.394437	-0.394483	-0.394443
9	-0.393813	-0.393813	-0.393821	-0.393831	-0.393845	-0.393862	-0.393870	-0.393832	-0.393637	-0.393175
10	-0.393828	-0.393828	-0.393828	-0.393830	-0.393836	-0.393847	-0.393860	-0.393852	-0.393710	-0.392821
11	-0.393813	-0.393813	-0.393821	-0.393831	-0.393845	-0.393862	-0.393870	-0.393832	-0.393637	-0.393175
12	-0.394036	-0.394036	-0.394069	-0.394116	-0.394177	-0.394255	-0.394348	-0.394437	-0.394483	-0.394443
13	-0.395276	-0.395276	-0.395357	-0.395468	-0.395617	-0.395816	-0.396080	-0.396426	-0.396889	-0.397582
14	-0.398716	-0.398716	-0.398839	-0.399010	-0.399246	-0.399572	-0.400024	-0.400659	-0.401586	-0.403048
15	-0.404870	-0.404870	-0.405000	-0.405183	-0.405439	-0.405799	-0.406307	-0.407033	-0.408096	-0.409706
16	-0.412880	-0.412880	-0.412982	-0.413125	-0.413327	-0.413612	-0.414019	-0.414602	-0.415448	-0.416693
17	-0.421550	-0.421550	-0.421612	-0.421700	-0.421826	-0.422004	-0.422261	-0.422633	-0.423180	-0.423998
18	-0.430000	-0.430000	-0.430027	-0.430065	-0.430120	-0.430199	-0.430315	-0.430488	-0.430752	-0.431161
19	-0.437687	-0.437687	-0.437687	-0.437687	-0.437687	-0.437687	-0.437687	-0.437687	-0.437687	-0.437687

Figure 10. Computed Dynamic Complementary Pressure Distribution

	P PRIME E -3									
1	-0.180761	-0.180761	-0.180761	-0.180761	-0.180761	-0.180761	-0.180761	-0.180761	-0.180761	-0.180761
2	-0.184882	-0.184879	-0.184876	-0.184873	-0.184868	-0.184861	-0.184854	-0.184844	-0.184831	-0.184814
3	-0.190170	-0.190164	-0.190156	-0.190145	-0.190133	-0.190117	-0.190096	-0.190071	-0.190039	-0.189999
4	-0.196294	-0.196282	-0.196267	-0.196248	-0.196224	-0.196194	-0.196156	-0.196108	-0.196049	-0.195973
5	-0.202689	-0.202671	-0.202649	-0.202620	-0.202585	-0.202542	-0.202487	-0.202418	-0.202331	-0.202222
6	-0.208962	-0.208938	-0.208907	-0.208868	-0.208818	-0.208758	-0.208680	-0.208584	-0.208463	-0.208313
7	-0.214759	-0.214728	-0.214688	-0.214638	-0.214577	-0.214501	-0.214407	-0.214290	-0.214145	-0.213966
8	-0.220357	-0.220292	-0.220212	-0.220114	-0.219992	-0.219845	-0.219670	-0.219469	-0.219246	-0.219025
9	-0.232194	-0.231916	-0.231564	-0.231115	-0.230539	-0.229797	-0.228830	-0.227557	-0.225855	-0.223438
10	-0.276772	-0.276274	-0.275674	-0.274959	-0.274120	-0.273152	-0.272066	-0.270893	-0.269700	-0.268809
11	-0.232200	-0.231923	-0.231570	-0.231121	-0.230545	-0.229802	-0.228834	-0.227562	-0.225858	-0.223438
12	-0.220360	-0.220296	-0.220217	-0.220116	-0.219995	-0.219848	-0.219673	-0.219470	-0.219246	-0.219025
13	-0.214760	-0.214728	-0.214689	-0.214640	-0.214579	-0.214503	-0.214408	-0.214291	-0.214146	-0.213966
14	-0.208960	-0.208936	-0.208905	-0.208867	-0.208818	-0.208757	-0.208680	-0.208584	-0.208464	-0.208313
15	-0.202691	-0.202673	-0.202650	-0.202622	-0.202588	-0.202545	-0.202489	-0.202419	-0.202332	-0.202222
16	-0.196283	-0.196272	-0.196257	-0.196238	-0.196216	-0.196188	-0.196152	-0.196105	-0.196047	-0.195973
17	-0.190174	-0.190167	-0.190160	-0.190149	-0.190136	-0.190120	-0.190099	-0.190073	-0.190040	-0.189999
18	-0.184885	-0.184883	-0.184880	-0.184876	-0.184871	-0.184865	-0.184856	-0.184846	-0.184832	-0.184814
19	-0.180761	-0.180761	-0.180761	-0.180761	-0.180761	-0.180761	-0.180761	-0.180761	-0.180761	-0.180761

Figure 11. Computed Complementary Pressure x_1 Gradient Distribution

C O M O C

3-DIMENSIONAL PARABOLIC NAVIER-STOKES OPTION

WING-FUSELAGE JUNCTURE FLOW.

LOCAL PRESSURE	.PSF.....	.PSI.....	.NT/M2.....	.TORR.....
0.0 E+00	0.21168E+04	0.14699E+02	0.10135E+06	0.76014E+03
LOCAL SOLUTION	.MACH. NO.	..DPDX1...	..ENERGY..	INT. VAR.
0.11201E+01	0.88615E-01	0.0 E+00	0.62664E+07	0.15600E+03
NWGEOM H'S	...H21....	...G22....	...G23....	....F1....
	0.10000E+01	0.0 E+00	0.0 E+00	0.0 E+00
NWGEOM H'S	...H31....	...G32....	...G33....	....G1....
	0.10000E+01	0.0 E+00	0.0 E+00	0.0 E+00
X1/LREF	.DX1/LREF.	.EPSILON..	.DX1M/LREF	REFL REYNOLDS NO
0.46400E-01	0.10000E-03	0.10000E-04	0.10000E-03	0.60480E+06

- X - X - X - X - X - X - X - X - X - X - X - X - X - X - X - X - X - X - X - X - X - X - X - X - X - X -

N- 1 N+ 1 PASSES 3 PRINT 2 OF 100

U1/UREF E 0

1	0.0	0.317980	0.389560	0.439870	0.487965	0.542509	0.614498	0.715576	0.843122	0.935620
2	0.0	0.315029	0.385976	0.436183	0.483851	0.537926	0.609472	0.709823	0.836501	0.928610
3	0.0	0.313201	0.383304	0.432923	0.480136	0.533665	0.604505	0.703893	0.829390	0.920865
4	0.0	0.311193	0.380540	0.429592	0.476302	0.529281	0.599406	0.697796	0.822068	0.912898
5	0.0	0.309382	0.377986	0.426495	0.472719	0.525148	0.594561	0.691961	0.815021	0.905212
6	0.0	0.308972	0.376869	0.424820	0.470522	0.522337	0.590932	0.687175	0.808752	0.897825
7	0.0	0.310386	0.377691	0.425125	0.470316	0.521516	0.589279	0.684331	0.804293	0.891723
8	0.0	0.312370	0.379277	0.426350	0.471185	0.521938	0.589102	0.683304	0.802087	0.888186
9	0.0	0.314052	0.380801	0.427613	0.472239	0.522790	0.589644	0.683367	0.801483	0.886723
10	0.0	0.314530	0.381423	0.428321	0.472756	0.523020	0.589835	0.683501	0.801481	0.886379
11	0.0	0.314052	0.380801	0.427613	0.472239	0.522790	0.589644	0.683367	0.801483	0.886723
12	0.0	0.312370	0.379277	0.426350	0.471185	0.521938	0.589102	0.683304	0.802087	0.888186
13	0.0	0.310386	0.377691	0.425125	0.470316	0.521516	0.589279	0.684331	0.804293	0.891723
14	0.0	0.308972	0.376869	0.424820	0.470522	0.522337	0.590932	0.687175	0.808752	0.897825
15	0.0	0.309382	0.377986	0.426495	0.472719	0.525148	0.594561	0.691961	0.815021	0.905212
16	0.0	0.311193	0.380540	0.429592	0.476302	0.529281	0.599406	0.697796	0.822068	0.912898
17	0.0	0.313201	0.383304	0.432923	0.480136	0.533665	0.604505	0.703893	0.829390	0.920865
18	0.0	0.315029	0.385976	0.436183	0.483851	0.537926	0.609472	0.709823	0.836501	0.928610
19	0.0	0.317980	0.389560	0.439870	0.487965	0.542509	0.614498	0.715576	0.843122	0.935620

Figure 12. Initialized Distribution For $\tilde{u}_1$ From Cole's Law

TKE / TKEREF E -2

1	0.0	0.002877	0.008812	0.032563	0.091832	0.198070	0.112638	0.066322	0.028146	0.0
2	0.0	0.002923	0.008915	0.032825	0.091896	0.195812	0.110747	0.065602	0.027780	0.0
3	0.0	0.003173	0.009344	0.033584	0.091992	0.193548	0.108872	0.064343	0.027315	0.0
4	0.0	0.003472	0.009866	0.034448	0.092238	0.191009	0.106917	0.063093	0.026831	0.0
5	0.0	0.003768	0.010342	0.035167	0.092223	0.188281	0.104939	0.061861	0.026355	0.0
6	0.0	0.004094	0.010784	0.035711	0.091761	0.184778	0.102562	0.060377	0.025715	0.0
7	0.0	0.004480	0.011237	0.036205	0.091138	0.181000	0.100057	0.058793	0.024946	0.0
8	0.0	0.004871	0.011687	0.036757	0.090831	0.178305	0.098264	0.057650	0.024373	0.0
9	0.0	0.005214	0.012104	0.037258	0.090993	0.176950	0.097307	0.057000	0.024012	0.0
10	0.0	0.005477	0.012550	0.037939	0.091241	0.176578	0.096927	0.057000	0.023907	0.0
11	0.0	0.005214	0.012104	0.037258	0.090993	0.176952	0.097308	0.057001	0.024012	0.0
12	0.0	0.004871	0.011687	0.036756	0.090832	0.178306	0.098264	0.057650	0.024373	0.0
13	0.0	0.004480	0.011238	0.036206	0.091138	0.181000	0.100057	0.058793	0.024946	0.0
14	0.0	0.004094	0.010784	0.035710	0.091760	0.184779	0.102561	0.060376	0.025715	0.0
15	0.0	0.003767	0.010341	0.035166	0.092224	0.188292	0.104938	0.061860	0.026355	0.0
16	0.0	0.003472	0.009867	0.034450	0.092242	0.191009	0.106914	0.063094	0.026831	0.0
17	0.0	0.003173	0.009344	0.033586	0.091990	0.193543	0.108872	0.064344	0.027315	0.0
18	0.0	0.002922	0.008915	0.032823	0.091890	0.195809	0.110748	0.065601	0.027780	0.0
19	0.0	0.002877	0.008812	0.032563	0.091832	0.198070	0.112638	0.066322	0.028146	0.0

Figure 13. Computed Initial Distribution Of Turbulence Kinetic Energy

DISS / DISSREF E -6

1	0.0	0.004313	0.009920	0.040414	0.126563	0.283152	0.091691	0.033115	0.007955	0.0
2	0.0	0.004304	0.009836	0.039854	0.123268	0.271190	0.087140	0.031894	0.007541	0.0
3	0.0	0.004614	0.010002	0.039086	0.117092	0.252769	0.080588	0.029389	0.006984	0.0
4	0.0	0.004982	0.010239	0.038309	0.110980	0.234082	0.074116	0.026966	0.006423	0.0
5	0.0	0.005341	0.010421	0.037473	0.105267	0.217500	0.068453	0.024867	0.005937	0.0
6	0.0	0.005784	0.010608	0.036660	0.099908	0.202353	0.063317	0.022954	0.005477	0.0
7	0.0	0.006379	0.010874	0.036063	0.095301	0.189198	0.058867	0.021280	0.005048	0.0
8	0.0	0.007018	0.011191	0.035799	0.092091	0.179619	0.055665	0.020074	0.004742	0.0
9	0.0	0.007588	0.011514	0.035662	0.090265	0.173381	0.053575	0.019273	0.004508	0.0
10	0.0	0.008012	0.011924	0.035943	0.089058	0.169632	0.052309	0.018980	0.004412	0.0
11	0.0	0.007588	0.011514	0.035662	0.090266	0.173384	0.053575	0.019273	0.004508	0.0
12	0.0	0.007018	0.011191	0.035799	0.092092	0.179620	0.055665	0.020074	0.004742	0.0
13	0.0	0.006379	0.010874	0.036064	0.095302	0.189197	0.058866	0.021280	0.005048	0.0
14	0.0	0.005783	0.010608	0.036658	0.099907	0.202354	0.063317	0.022954	0.005477	0.0
15	0.0	0.005341	0.010420	0.037473	0.105268	0.217520	0.068453	0.024866	0.005937	0.0
16	0.0	0.004982	0.010239	0.038311	0.110987	0.234081	0.074113	0.026967	0.006423	0.0
17	0.0	0.004614	0.010002	0.039088	0.117090	0.252759	0.080589	0.029389	0.006984	0.0
18	0.0	0.004303	0.009836	0.039853	0.123258	0.271184	0.087141	0.031894	0.007541	0.0
19	0.0	0.004313	0.009920	0.040414	0.126563	0.283152	0.091691	0.033115	0.007955	0.0

Figure 14. Computed Initial Distribution Of Isotropic Dissipation

	V2/UREF E -1									
1	0.0	0.0	0.0	0.0	0.0	0.0	0.0	0.0	0.0	0.0
2	0.0	0.004999	0.010774	-0.000338	-0.012542	-0.028331	-0.046111	-0.068867	-0.097088	-0.126414
3	0.0	0.008102	0.016203	-0.005716	-0.029203	-0.059705	-0.094377	-0.138222	-0.193715	-0.251050
4	0.0	0.010101	0.019173	-0.011869	-0.046171	-0.090288	-0.141022	-0.205524	-0.286893	-0.370978
5	0.0	0.010793	0.018581	-0.021192	-0.065935	-0.123000	-0.189662	-0.274804	-0.382325	-0.493262
6	0.0	0.011233	0.017514	-0.030065	-0.083974	-0.152620	-0.233645	-0.337670	-0.469336	-0.605209
7	0.0	0.011901	0.017514	-0.036485	-0.097974	-0.176243	-0.269533	-0.389960	-0.543170	-0.702555
8	0.0	0.012991	0.019464	-0.038248	-0.103700	-0.187088	-0.286824	-0.414909	-0.578134	-0.749181
9	0.0	0.013207	0.017837	-0.047670	-0.122888	-0.218990	-0.337490	-0.494134	-0.693797	-0.897241
10	0.0	0.013473	0.018197	-0.048629	-0.125364	-0.223403	-0.344292	-0.504095	-0.707784	-0.915329
11	0.0	0.013740	0.018557	-0.049590	-0.127841	-0.227818	-0.351096	-0.514056	-0.721771	-0.933417
12	0.0	0.014232	0.021324	-0.041903	-0.113608	-0.204961	-0.314226	-0.454548	-0.633367	-0.820754
13	0.0	0.013964	0.020549	-0.042811	-0.114961	-0.206801	-0.316265	-0.457572	-0.637345	-0.824362
14	0.0	0.014465	0.022554	-0.038718	-0.108140	-0.196539	-0.300887	-0.434866	-0.604415	-0.779384
15	0.0	0.015825	0.027240	-0.031088	-0.096700	-0.180380	-0.278137	-0.402994	-0.560667	-0.723347
16	0.0	0.017921	0.034018	-0.021056	-0.081911	-0.160181	-0.250194	-0.364628	-0.508991	-0.658169
17	0.0	0.019486	0.038969	-0.013744	-0.070228	-0.143588	-0.226973	-0.332420	-0.465865	-0.603719
18	0.0	0.021640	0.046636	-0.001467	-0.054300	-0.122655	-0.199638	-0.298147	-0.420317	-0.547275
19	0.0	0.026494	0.055768	-0.001276	-0.047603	-0.115804	-0.193370	-0.281360	-0.392376	-0.518875

Figure 15. Computed Solution Of Transverse Plane Vertical Velocity $\tilde{v}_2$

	V3/UREF E -1									
1	0.0	0.026495	0.055770	-0.001274	-0.047601	-0.115802	-0.193368	-0.281358	-0.392374	-0.518873
2	0.0	0.021643	0.046642	-0.001464	-0.054297	-0.122646	-0.199620	-0.298131	-0.420300	-0.547258
3	0.0	0.019486	0.038968	-0.013748	-0.070232	-0.143590	-0.226975	-0.332423	-0.465883	-0.603774
4	0.0	0.017920	0.034015	-0.021058	-0.081914	-0.160185	-0.250195	-0.364631	-0.508993	-0.658172
5	0.0	0.015827	0.027248	-0.031077	-0.096690	-0.180372	-0.278129	-0.402984	-0.560658	-0.723340
6	0.0	0.014465	0.022554	-0.038717	-0.108138	-0.196537	-0.300878	-0.434836	-0.604390	-0.779361
7	0.0	0.013965	0.020551	-0.042811	-0.114961	-0.206800	-0.316264	-0.457571	-0.637344	-0.824363
8	0.0	0.014232	0.021324	-0.041902	-0.113607	-0.204961	-0.314225	-0.454547	-0.633365	-0.820753
9	0.0	0.013740	0.018556	-0.049592	-0.127843	-0.227820	-0.351098	-0.514058	-0.721771	-0.933418
10	0.0	0.013473	0.018197	-0.048629	-0.125364	-0.223403	-0.344292	-0.504095	-0.707784	-0.915329
11	0.0	0.013207	0.017838	-0.047668	-0.122887	-0.218988	-0.337488	-0.494133	-0.693797	-0.897241
12	0.0	0.012991	0.019464	-0.038249	-0.103701	-0.187088	-0.286825	-0.414910	-0.578136	-0.749182
13	0.0	0.011901	0.017513	-0.036486	-0.097975	-0.176244	-0.269534	-0.389962	-0.543172	-0.702556
14	0.0	0.011233	0.017514	-0.030066	-0.083976	-0.152622	-0.233654	-0.337695	-0.469358	-0.605230
15	0.0	0.010791	0.018575	-0.021200	-0.065942	-0.123005	-0.189668	-0.274810	-0.382331	-0.493266
16	0.0	0.010101	0.019174	-0.011868	-0.046169	-0.090286	-0.141021	-0.205522	-0.286892	-0.370976
17	0.0	0.008103	0.016204	-0.005715	-0.029201	-0.059705	-0.094377	-0.138223	-0.193710	-0.251031
18	0.0	0.004999	0.010773	-0.000339	-0.012543	-0.028332	-0.046115	-0.068869	-0.097090	-0.126416
19	0.0	0.0	0.0	0.0	0.0	0.0	0.0	0.0	0.0	0.0

Figure 16. Computed Solution Of Transverse Plane Horizontal Velocity $\tilde{v}_3$

The 3DPNS solution is initialized with $\tilde{u}_1$,k, ε, p_c, and four small (10^{-4}) integration steps are taken forward to generate sufficient $\tilde{u}_1$ data to evaluate axial derivatives using a second-order accurate backwards difference formula. At this station, an estimation of $\tilde{v}_\ell$ is computed by direct integration of the continuity equation (24) in the form

$$\frac{\partial(\bar{\rho}\tilde{v}_n)}{\partial x_n} = - \frac{\partial(\bar{\rho}\tilde{u}_1)}{\partial x_1} \tag{75}$$

In equation (75), x_n is the coordinate parallel to a node "column," and related to x_ℓ by the familiar direction cosines $a_{n\ell}$, i.e.

$$x_n = a_{n\ell}x_\ell \qquad 2 \leq \ell \leq 3 \tag{76}$$

The solution to equation (75) is the scalar component of $\bar{\rho}\tilde{v}_\ell$ parallel to the node column; hence, the Cartesian components are determined as

$$\tilde{v}_\ell = a_{\ell n}\tilde{v}_n \tag{77}$$

The $\tilde{v}_\ell$ distributions are computed as this for the next four stations, and are inserted non-iteratively in 3DPNS solution for $\tilde{u}_1$, k and ε. Then, at stations 8-10, the transverse velocity solutions from equation (75) are iterated directly with $\tilde{u}_1$, such that a divergence-free three-dimensional velocity field $\bar{\rho}\tilde{u}_i$ becomes established. Hence, the transverse momentum equations for $\tilde{v}_\ell$ are initialized with $\tilde{u}_\ell$ at station 11, and the solution of the complete 3DPNS system initialized. Figures 15-16 show the computed $\tilde{v}_\ell$ distributions at station 11.

This completes the program generated solution initiation sequence which is descripted in program input terms in the following section. The last remaining requirement is specification of the turbulence model constants. The various coefficients are all NAMELIST input; their specification for the test case are, C_{ϕ_1} = 2.8, C_{ϕ_2} = 0.45, C_k = 1.0, C_ε = 1.3, C_ε^1 = 1.44, C_ε^2 = 1.92, and C_ν = 0.09.

Test Case Results

Upon completion of the 3DPNS solution initiation, a specified number (four) of integration steps are taken at $\Delta x = 10^{-4}$, to homogenize the $\tilde{v}_\ell$ 3DPNS solutions and initialize the predictor-corrector sequence for perturbation velocities and particular pressure. Figures 17-18 show the resultant computed perturbation velocity distributions, while Figure 19 presents the particular pressure distribution at $x_1/C \approx 0.046$.

Figure 20 is a victor plot of the transverse velocity distribution at this station. Note that the initiation procedure induces no tendency to roll up the transverse field. Figure 21 shows the corresponding computed particular pressure, and dynamic complementary pressure distributions parallel to the corner bisector and parallel to one wall. The corresponding transverse plane gradients of particular pressure are almost an order of magnitude larger than those associated with the dynamic complementary pressure. However, absolute level of particular pressure is only ~ 2% of the dynamic complementary pressure.

Figure 22 is the vector plot of transverse velocity distribution computed at $x_1/C = 0.12$, the station at which the 3DPNS computation was stopped. The combined action of the Reynolds stress distribution and the transverse plane pressure gradient has induced a reversed flow region emanating from the corner. A modest rotational region separates this reversed flow from the axial pressure gradient-dominated mass influx into the corner. The location of this region proceeds in a symmetric fashion away from the corner and parallel to the main diagonal. There is also an induced flow parallel to both walls and away from the corner. The net action on the predominant velocity $\tilde{u}_1$ is to cause an undulation in the profile parallel to the wall, with the minima at the corner and at the lateral outflow boundaries. Figure 23 is the output from COMOC III for the computed $\tilde{u}_1$ distribution, and Figure 24 is the corresponding particular pressure distribution.

Additional output from the code includes all other velocity and pressure fields, the turbulence kinetic energy and dissipation distributions, as well as integral evaluation of skin friction and displacement and momentum thicknesses. These boundary layer integral parameters are evaluated by integrating parallel to node "columns" of the discretization. Upon a restart specification, the computation of the six components of Reynolds stress $-\overline{u_i u_j}$ using equations (30) can be commanded. Figure 25 is a plot of the distributions of $\overline{u_i u_j}$ at $x_1/C = 0.12$ along the mid-discretization node-row parallel to the wall. This is the transverse location of the extremum boundary layer shear stresses $\overline{u_1' u_2'}$ and $\overline{u_1' u_3'}$ on the farfield outflow boundaries. Both are characterized by relatively flat plateaus with a sharp decrease of two orders of magnitude about the corner bisector. The transverse plane shear stress $\overline{u_2' u_3'}$ is up to ten times smaller than these and exhibits a smooth increase to an extremum at the domain diagonal. The three normal stresses are nominally uniform with the x_1-component about twice the level of the transverse plane components. Figure 26 is a reproduction of the COMOC III computation of the complete distribution of $\overline{u_i' u_j'}$ at this station.

	V2PR	E -3								
1	0.0	-0.000433	-0.001045	-0.002551	-0.007716	-0.016988	-0.030196	-0.049210	-0.074996	-0.094088
2	0.0	0.000279	0.000667	0.000621	-0.001222	-0.005805	-0.012330	-0.021677	-0.035377	-0.046243
3	0.0	0.000692	0.001662	0.002148	0.002420	0.002175	0.001841	0.001432	-0.000215	-0.002108
4	0.0	0.000539	0.001301	0.000818	-0.000085	-0.000871	-0.001968	-0.003493	-0.005636	-0.006888
5	0.0	0.000163	0.000417	-0.000322	-0.001373	-0.001839	-0.002760	-0.004476	-0.007431	-0.009608
6	0.0	-0.000627	-0.001465	-0.001318	-0.000777	0.000781	0.001670	0.000764	-0.003327	-0.009464
7	0.0	-0.001157	-0.002699	-0.000123	0.005007	0.013476	0.020879	0.023112	0.018679	0.004240
8	0.0	-0.002461	0.002665	0.012990	0.030177	0.051715	0.074625	0.090334	0.091285	0.076247
9	0.0	-0.001954	0.005770	0.019225	0.041663	0.072307	0.109966	0.145730	0.161973	0.137295
10	0.0	-0.084981	-0.158370	-0.137365	-0.098243	-0.053821	0.018805	0.105838	0.139277	0.110343
11	0.0	-0.044674	-0.197404	-0.159977	-0.099848	-0.044898	0.025089	0.111848	0.115704	0.093566
12	0.0	-0.010000	-0.039568	0.021215	0.085674	0.119127	0.159996	0.208333	0.176011	0.117417
13	0.0	-0.057040	0.007822	0.118038	0.212381	0.241616	0.257454	0.278556	0.221236	0.165344
14	0.0	-0.088468	-0.005757	0.143611	0.250859	0.282420	0.286408	0.291220	0.223022	0.156338
15	0.0	-0.098571	-0.027356	0.129422	0.247482	0.285768	0.285674	0.285336	0.215580	0.146267
16	0.0	-0.070725	-0.025284	0.109427	0.230513	0.273846	0.273316	0.272320	0.205437	0.138710
17	0.0	-0.031275	-0.004718	0.100091	0.214628	0.263213	0.262668	0.258689	0.193300	0.131877
18	0.0	0.029361	0.044267	0.120474	0.220227	0.263744	0.264890	0.259579	0.201941	0.125475
19	0.0	0.015698	0.015819	0.028277	0.069576	0.088905	0.089729	0.091219	0.087218	0.067685

Figure 17. Computed Transverse Plane Vertical Perturbation Velocity $p\tilde{v}_2$

	V3PR	E -3								
1	0.0	0.016248	0.016370	0.028696	0.070017	0.089267	0.090102	0.091607	0.087316	0.067695
2	0.0	0.030853	0.045600	0.121687	0.221362	0.264609	0.265774	0.260121	0.202013	0.125445
3	0.0	-0.030398	-0.003881	0.100967	0.215151	0.263408	0.262869	0.258734	0.193293	0.131898
4	0.0	-0.070551	-0.025064	0.109699	0.230563	0.273905	0.273372	0.272360	0.205478	0.138746
5	0.0	-0.098831	-0.027539	0.129339	0.247531	0.286000	0.285889	0.285527	0.215744	0.146407
6	0.0	-0.088715	-0.005882	0.143669	0.251150	0.282802	0.286787	0.291598	0.223344	0.156568
7	0.0	-0.057142	0.007851	0.118224	0.212691	0.241950	0.257809	0.278949	0.221499	0.165455
8	0.0	-0.010049	-0.039574	0.021273	0.085825	0.119293	0.160182	0.208519	0.176057	0.117411
9	0.0	-0.044782	-0.197513	-0.159983	-0.099777	-0.044839	0.025141	0.111875	0.115640	0.093498
10	0.0	-0.085003	-0.158379	-0.137315	-0.098205	-0.053798	0.018812	0.105801	0.139142	0.110158
11	0.0	-0.001953	0.005773	0.019230	0.041657	0.072285	0.109916	0.145623	0.161778	0.137007
12	0.0	-0.002463	0.002660	0.012973	0.030149	0.051667	0.074543	0.090201	0.091075	0.076044
13	0.0	-0.001154	-0.002690	-0.000115	0.005013	0.013469	0.020859	0.023082	0.018641	0.004222
14	0.0	-0.000624	-0.001457	-0.001302	-0.000745	0.000816	0.001716	0.000833	-0.003207	-0.009315
15	0.0	0.000159	0.000409	-0.000334	-0.001386	-0.001839	-0.002742	-0.004433	-0.007352	-0.009517
16	0.0	0.000530	0.001279	0.000778	-0.000148	-0.000928	-0.002019	-0.003538	-0.005679	-0.006940
17	0.0	0.000683	0.001640	0.002112	0.002365	0.002098	0.001731	0.001273	-0.000391	-0.002280
18	0.0	0.000282	0.000674	0.000636	-0.001196	-0.005782	-0.012312	-0.021664	-0.035361	-0.046216
19	0.0	-0.000418	-0.001010	-0.002493	-0.007626	-0.016860	-0.030014	-0.048947	-0.074703	-0.093793

Figure 18. Computed Transverse Plane Horizontal Perturbation Velocity $p\tilde{v}_3$

	PP	E -1								
1	0.000058	0.0	0.0	0.0	0.0	0.0	0.0	0.0	0.0	0.0
2	0.072187	0.071990	0.071688	0.071428	0.070057	0.066633	0.060134	0.048442	0.029096	0.0
3	0.085619	0.085466	0.085236	0.084970	0.083390	0.079463	0.071900	0.058000	0.034899	0.0
4	0.099677	0.099469	0.099186	0.098709	0.096672	0.091891	0.082882	0.066501	0.039641	0.0
5	0.117920	0.117583	0.117138	0.116284	0.113536	0.107533	0.096515	0.076857	0.045252	0.0
6	0.142594	0.142000	0.141200	0.139712	0.135896	0.128165	0.114403	0.090404	0.052591	0.0
7	0.176587	0.175540	0.174105	0.171625	0.166262	0.156133	0.138635	0.108812	0.062645	0.0
8	0.220919	0.219305	0.217071	0.213397	0.206214	0.193251	0.171169	0.133688	0.075521	0.0
9	0.268648	0.266838	0.264390	0.260423	0.252812	0.239087	0.215138	0.171970	0.097714	0.0
10	0.300817	0.299149	0.297140	0.294063	0.288397	0.278293	0.260164	0.223846	0.155476	0.0
11	0.268643	0.266833	0.264385	0.260419	0.252808	0.239084	0.215135	0.171968	0.097713	0.0
12	0.220909	0.219295	0.217061	0.213388	0.206206	0.193246	0.171165	0.133686	0.075520	0.0
13	0.176585	0.175539	0.174103	0.171624	0.166260	0.156132	0.138634	0.108811	0.062645	0.0
14	0.142594	0.141999	0.141199	0.139710	0.135894	0.128163	0.114401	0.090403	0.052590	0.0
15	0.117912	0.117575	0.117130	0.116277	0.113530	0.107527	0.096510	0.076854	0.045250	0.0
16	0.099681	0.099473	0.099190	0.098712	0.096676	0.091894	0.082884	0.066502	0.039642	0.0
17	0.085622	0.085470	0.085240	0.084974	0.083394	0.079466	0.071903	0.058002	0.034900	0.0
18	0.072184	0.071986	0.071685	0.071425	0.070054	0.066631	0.060132	0.048440	0.029095	0.0
19	0.000058	0.0	0.0	0.0	0.0	0.0	0.0	0.0	0.0	0.0

Figure 19. Computed Particular Pressure Distribution p_p

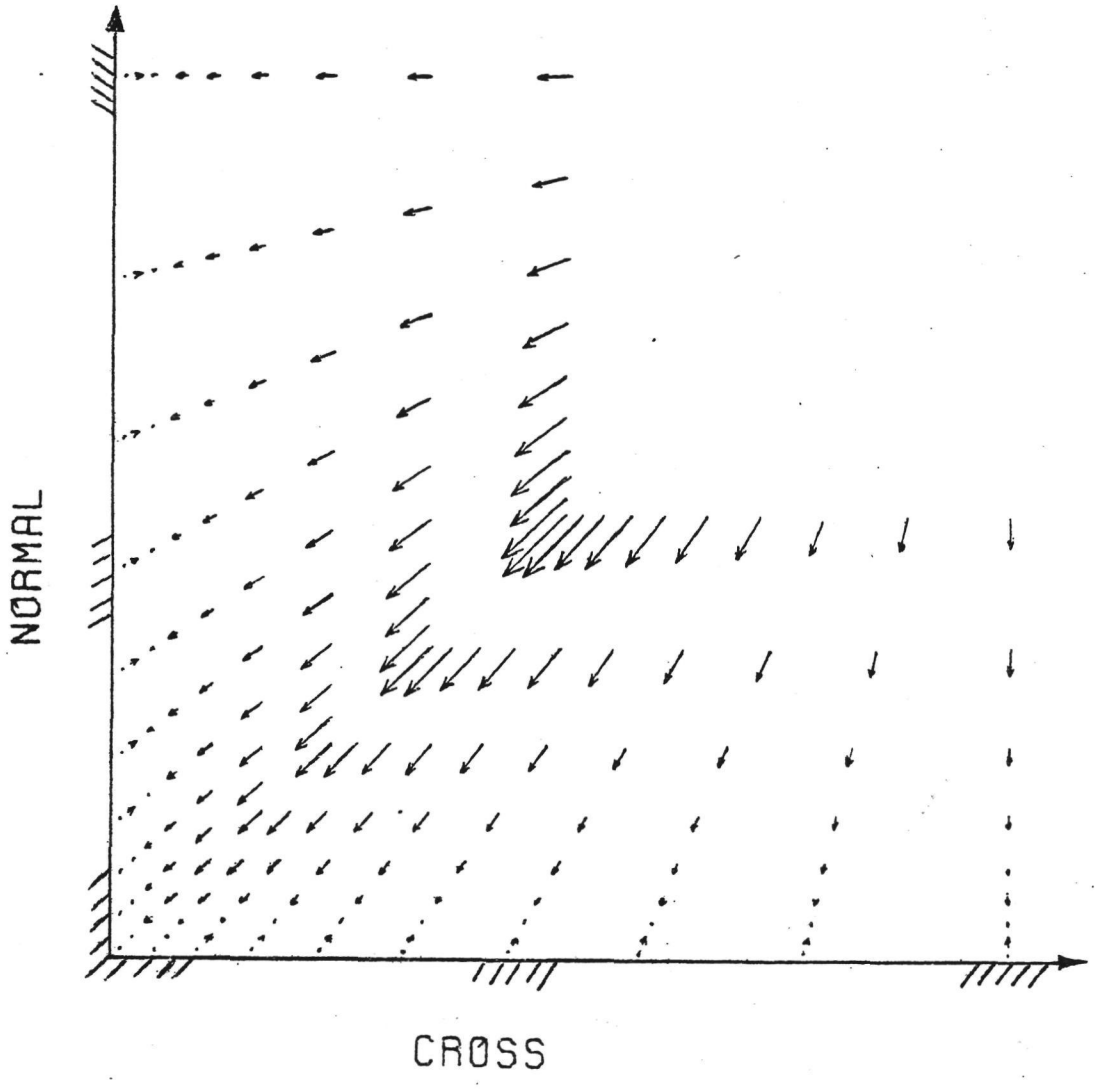

Figure 20. Transverse Plane Velocity Vector Distribution, Initial

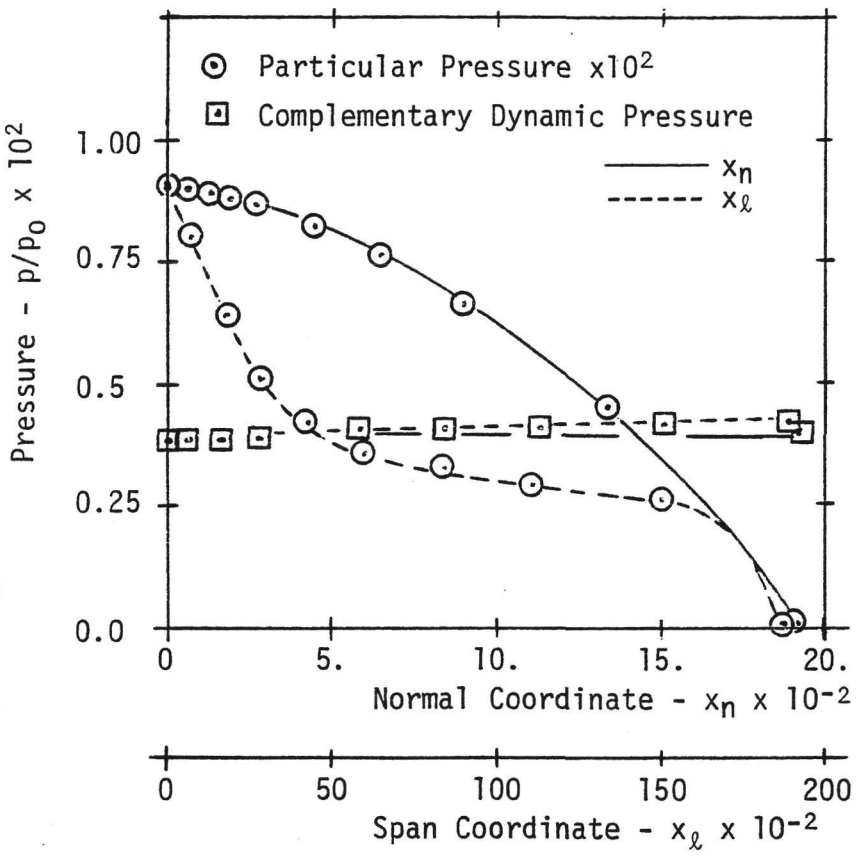

Figure 21. Computed Initial Particular and Complementary Dynamic Pressure Distributions on Transverse Plane

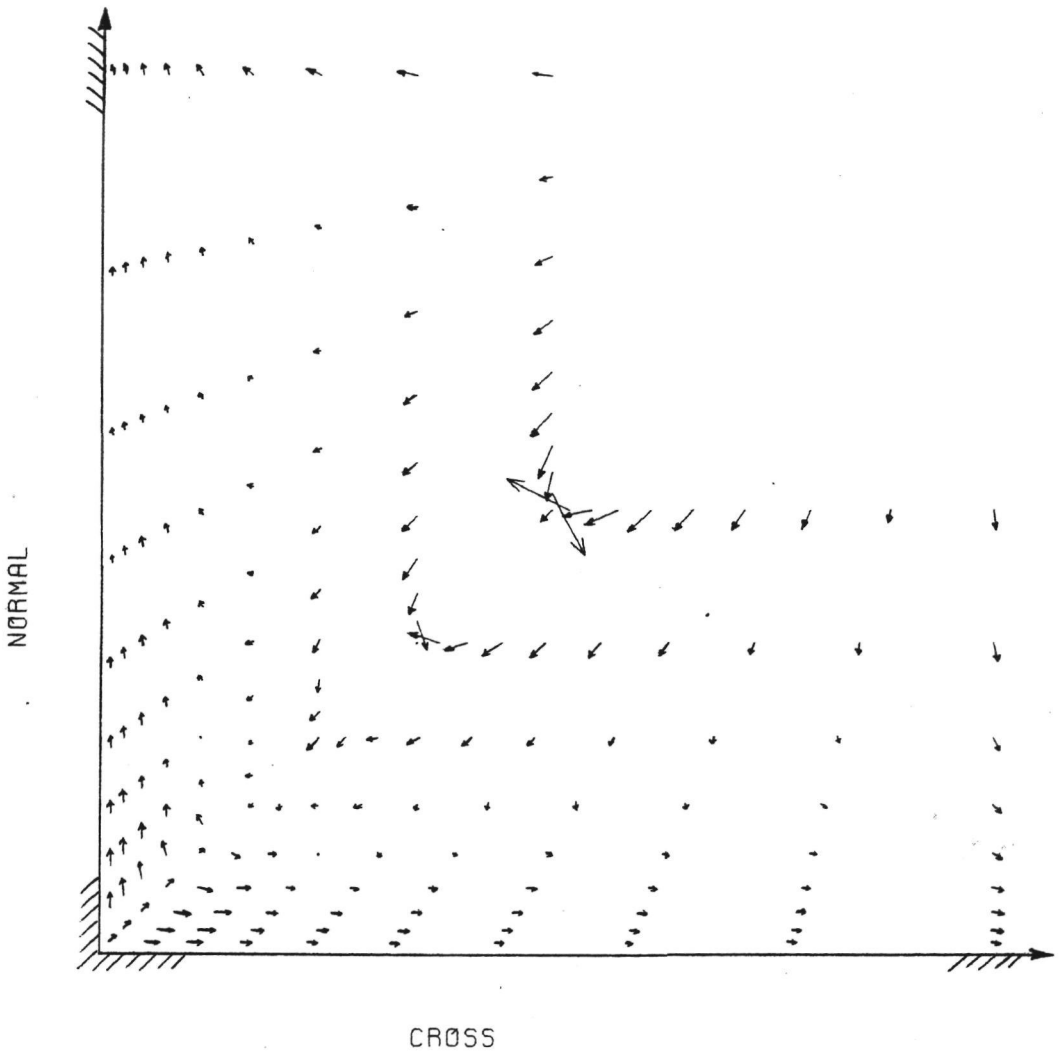

Figure 22. Transverse Plane Velocity Vector Distribution, $x_1/C = 0.12$

X1/LREF	.DX1/LREF.	.EPSILON..	.DX1M/LREF REFL	REYNOLDS NO
0.11799E+00	0.22000E-02	0.10000E-04	0.10000E-03	0.60480E+06

N-	N+	PASSES	PRINT	OF
39	75	449	4	100

	U1/UREF E 1								
1	0.0	0.037770	0.054401	0.061203	0.066239	0.073264	0.078624	0.088485	0.098577	0.105865
2	0.0	0.037577	0.052649	0.059008	0.065401	0.072231	0.078551	0.088760	0.098256	0.105939
3	0.0	0.039890	0.055005	0.061031	0.066830	0.073103	0.079269	0.089273	0.098545	0.106345
4	0.0	0.041561	0.056209	0.062134	0.067739	0.073999	0.080136	0.089962	0.098846	0.106414
5	0.0	0.043511	0.057435	0.062970	0.068759	0.074881	0.081065	0.090784	0.099324	0.106744
6	0.0	0.045826	0.058138	0.064083	0.070334	0.075898	0.082150	0.091641	0.099907	0.107109
7	0.0	0.043952	0.055319	0.063248	0.070676	0.076038	0.082451	0.092098	0.100153	0.107123
8	0.0	0.041043	0.052665	0.061647	0.070101	0.075044	0.081071	0.090840	0.099384	0.106985
9	0.0	0.038887	0.050776	0.063714	0.072894	0.077996	0.083162	0.091984	0.098646	0.104211
10	0.0	0.024010	0.035974	0.046417	0.058052	0.072459	0.081751	0.091397	0.098733	0.107322
11	0.0	0.038907	0.050796	0.063728	0.072899	0.077996	0.083163	0.091984	0.098645	0.104210
12	0.0	0.041079	0.052696	0.061668	0.070106	0.075046	0.081072	0.090841	0.099385	0.106985
13	0.0	0.043977	0.055337	0.063258	0.070677	0.076037	0.082451	0.092097	0.100153	0.107123
14	0.0	0.045852	0.058156	0.064055	0.070338	0.075899	0.082150	0.091641	0.099907	0.107109
15	0.0	0.043542	0.057456	0.062985	0.068767	0.074883	0.081066	0.090785	0.099324	0.106743
16	0.0	0.041587	0.056225	0.062144	0.067742	0.073998	0.080136	0.089961	0.098846	0.106414
17	0.0	0.039939	0.055040	0.061056	0.066844	0.073106	0.079271	0.089275	0.098546	0.106345
18	0.0	0.037596	0.052661	0.059016	0.065406	0.072231	0.078550	0.088757	0.098255	0.105939
19	0.0	0.037775	0.054402	0.061203	0.066239	0.073264	0.078625	0.088485	0.098577	0.105865

Figure 23. Computed $\tilde{u}_1$ Velocity Distribution, $x_1/C = 0.12$

	PP E -1									
1	0.000071	0.0	0.0	0.0	0.0	0.0	0.0	0.0	0.0	0.0
2	0.027607	0.027549	0.027473	0.027374	0.027214	0.026522	0.024940	0.021277	0.013282	0.0
3	0.024496	0.024469	0.024393	0.024262	0.024032	0.023481	0.022164	0.019103	0.012287	0.0
4	0.033593	0.033418	0.033122	0.032683	0.032009	0.030770	0.028417	0.023784	0.014967	0.0
5	0.060064	0.059417	0.058430	0.057016	0.054909	0.051523	0.046098	0.036905	0.021831	0.0
6	0.128112	0.126370	0.123840	0.120236	0.114888	0.106763	0.094344	0.074482	0.043215	0.0
7	0.241694	0.238522	0.234035	0.227652	0.218377	0.204556	0.183348	0.148947	0.091629	0.0
8	0.374480	0.370127	0.363946	0.355211	0.342728	0.324570	0.297687	0.254841	0.178015	0.0
9	0.495177	0.490841	0.484723	0.476459	0.464858	0.447869	0.422800	0.388900	0.320462	0.0
10	0.566291	0.562244	0.556356	0.548425	0.537391	0.519995	0.494298	0.465266	0.405306	0.0
11	0.495195	0.490859	0.484743	0.476480	0.464881	0.447894	0.422823	0.388923	0.320483	0.0
12	0.374492	0.370139	0.363956	0.355220	0.342735	0.324576	0.297692	0.254847	0.178021	0.0
13	0.241708	0.238536	0.234046	0.227662	0.218384	0.204561	0.183352	0.148950	0.091631	0.0
14	0.128139	0.126396	0.123864	0.120259	0.114909	0.106781	0.094358	0.074493	0.043220	0.0
15	0.060078	0.059431	0.058443	0.057027	0.054917	0.051528	0.046100	0.036905	0.021830	0.0
16	0.033602	0.033428	0.033131	0.032690	0.032015	0.030775	0.028420	0.023785	0.014967	0.0
17	0.024511	0.024484	0.024406	0.024273	0.024039	0.023484	0.022163	0.019099	0.012281	0.0
18	0.027543	0.027485	0.027409	0.027309	0.027148	0.026458	0.024879	0.021227	0.013252	0.0
19	0.000071	0.0	0.0	0.0	0.0	0.0	0.0	0.0	0.0	0.0

Figure 24. Computed Particular Pressure Distribution, $x_1/C = 0.12$

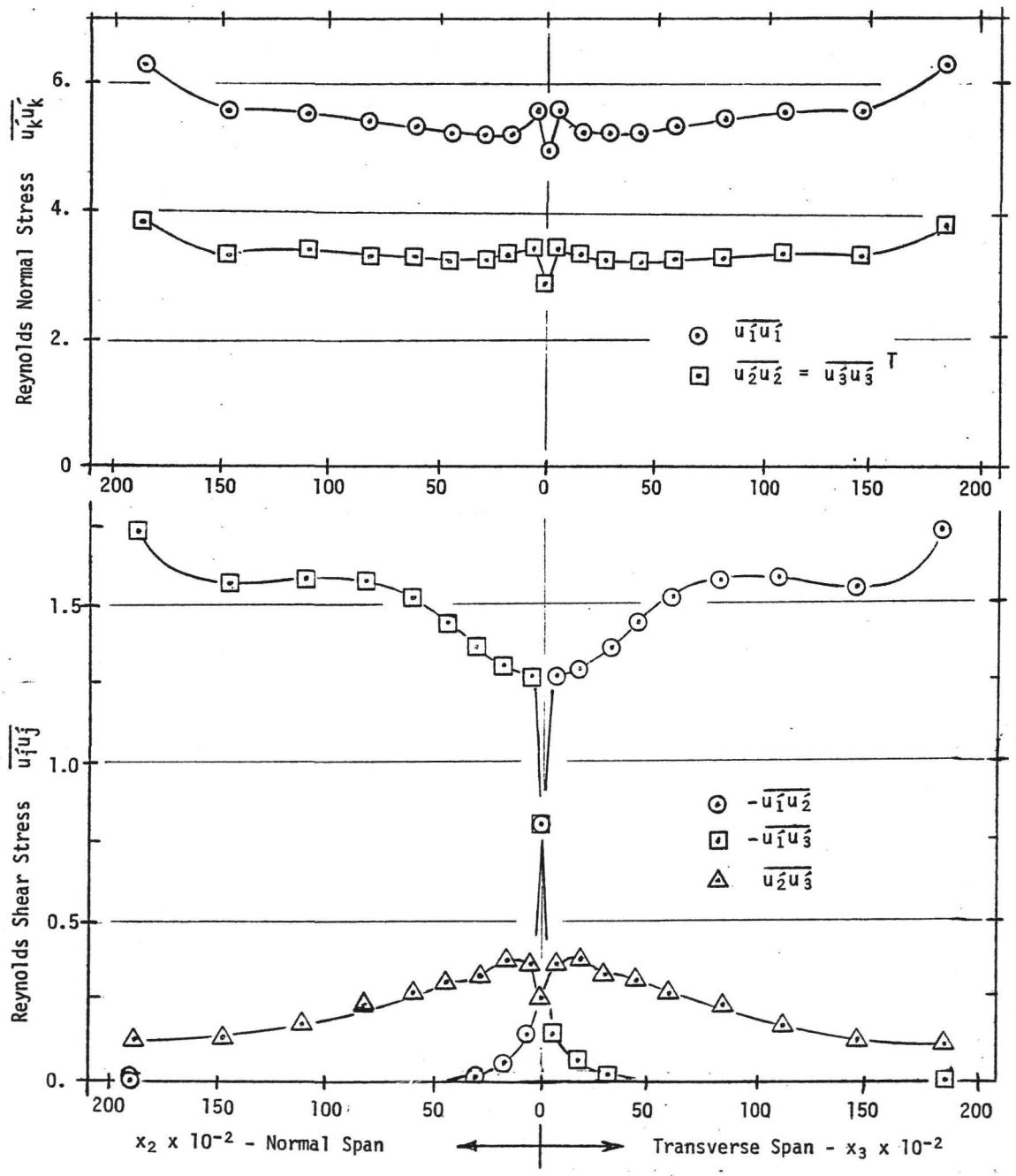

Figure 25. Computed Reynolds Stress Distributions Along Mid-Discretization Node Row of Juncture Region, $x_1/C = 0.12$

U1U2 * E 2

REYNOLD'S STRESS.

1	0.0	-0.000003	-0.000280	-0.000634	-0.000139	-0.000103	-0.000044	0.000012	-0.000026	0.0
2	0.0	0.000016	0.000098	0.000219	0.000054	0.000027	0.000050	0.000027	0.000008	0.0
3	0.0	0.000069	0.000509	0.000509	0.000110	0.000126	0.000113	0.000068	0.000062	0.0
4	0.0	0.000090	0.000537	0.000511	0.000124	0.000166	0.000156	0.000099	0.000083	0.0
5	0.0	0.000158	0.000605	0.000449	0.000179	0.000239	0.000219	0.000140	0.000163	0.0
6	0.0	0.000015	-0.000474	-0.000113	0.000095	0.000164	0.000161	0.000122	0.000171	0.0
7	0.0	-0.000433	-0.001544	-0.000194	-0.000051	-0.000124	-0.000171	-0.000103	-0.000117	0.0
8	0.0	-0.000332	-0.001136	-0.000077	0.000138	0.000413	0.000290	0.000055	-0.000239	0.0
9	0.0	-0.002861	-0.015763	-0.003904	-0.003612	-0.001360	-0.000226	-0.000097	-0.000030	0.0
10	0.0	-0.006257	-0.028692	-0.055954	-0.016124	-0.008158	-0.007224	-0.004147	-0.002422	0.0
11	0.0	-0.198566	-0.240015	-0.031245	-0.017952	-0.012931	-0.012685	-0.006970	-0.004133	0.0
12	0.0	-0.104103	-0.099484	-0.015086	-0.008004	-0.013108	-0.013552	-0.008134	-0.006503	0.0
13	0.0	-0.166439	-0.129982	-0.015358	-0.010719	-0.013713	-0.013253	-0.007889	-0.014093	0.0
14	0.0	-0.161231	-0.128053	-0.028602	-0.012123	-0.014463	-0.013264	-0.008185	-0.009696	0.0
15	0.0	-0.134994	-0.161031	-0.071447	-0.014469	-0.015348	-0.013724	-0.008779	-0.008918	0.0
16	0.0	-0.111139	-0.166334	-0.086309	-0.015956	-0.015800	-0.013964	-0.009262	-0.008438	0.0
17	0.0	-0.088874	-0.155244	-0.080859	-0.015157	-0.015893	-0.014301	-0.009630	-0.008100	0.0
18	0.0	-0.070088	-0.141929	-0.087450	-0.015766	-0.015727	-0.014263	-0.010139	-0.007961	0.0
19	0.0	-0.093742	-0.210883	-0.110072	-0.019857	-0.017506	-0.014877	-0.009016	-0.007189	0.0

a. $\overline{u_1' u_2'}$ Shear Stress

U1U3 * E 2

REYNOLD'S STRESS.

1	0.0	-0.093741	-0.211051	-0.110162	-0.019879	-0.017506	-0.014878	-0.009016	-0.007192	0.0
2	0.0	-0.069985	-0.142039	-0.087583	-0.015791	-0.015729	-0.014264	-0.010138	-0.007963	0.0
3	0.0	-0.088591	-0.155444	-0.081122	-0.015189	-0.015896	-0.014303	-0.009631	-0.008102	0.0
4	0.0	-0.111000	-0.166570	-0.086503	-0.015992	-0.015802	-0.013964	-0.009261	-0.008440	0.0
5	0.0	-0.134764	-0.161240	-0.071614	-0.014492	-0.015348	-0.013725	-0.008779	-0.008920	0.0
6	0.0	-0.161073	-0.128272	-0.028645	-0.012132	-0.014462	-0.013264	-0.008185	-0.009699	0.0
7	0.0	-0.166200	-0.130137	-0.015376	-0.010720	-0.013712	-0.013253	-0.007888	-0.014103	0.0
8	0.0	-0.103798	-0.099514	-0.015082	-0.007998	-0.013106	-0.013553	-0.008134	-0.006503	0.0
9	0.0	-0.198336	-0.240034	-0.031271	-0.017981	-0.012932	-0.012685	-0.006971	-0.004134	0.0
10	0.0	-0.006262	-0.028706	-0.055994	-0.016129	-0.008158	-0.007224	-0.004147	-0.002422	0.0
11	0.0	-0.002870	-0.015789	-0.003906	-0.003611	-0.001361	-0.000226	-0.000097	-0.000030	0.0
12	0.0	-0.000333	-0.001138	-0.000078	0.000139	0.000413	0.000290	0.000055	-0.000239	0.0
13	0.0	-0.000433	-0.001538	-0.000193	-0.000051	-0.000123	-0.000170	-0.000102	-0.000117	0.0
14	0.0	0.000015	-0.000474	-0.000113	0.000094	0.000164	0.000161	0.000122	0.000171	0.0
15	0.0	0.000158	0.000605	0.000448	0.000179	0.000239	0.000219	0.000140	0.000163	0.0
16	0.0	0.000090	0.000535	0.000511	0.000124	0.000166	0.000156	0.000099	0.000083	0.0
17	0.0	0.000069	0.000509	0.000506	0.000110	0.000126	0.000113	0.000068	0.000062	0.0
18	0.0	0.000017	0.000102	0.000224	0.000055	0.000027	0.000050	0.000027	0.000009	0.0
19	0.0	-0.000003	-0.000277	-0.000631	-0.000139	-0.000103	-0.000044	0.000012	-0.000026	0.0

b. $\overline{u_1' u_3'}$ Shear Stress

Figure 26. Computed Reynolds Stress Distributions, $x_1/C = 0.12$

U2U3 * E 2

REYNOLD'S STRESS.

1	0.0	-0.004824	-0.010829	-0.005022	0.000566	0.001157	0.000924	0.000569	0.000663	0.0
2	0.0	-0.001466	-0.000369	0.001809	0.000804	0.001228	0.001020	0.000736	0.000761	0.0
3	0.0	0.000573	0.004666	0.003888	0.001055	0.001656	0.001254	0.000803	0.000841	0.0
4	0.0	0.000514	0.005389	0.004442	0.001476	0.002292	0.001784	0.001153	0.001376	0.0
5	0.0	0.002917	0.008031	0.003803	0.001742	0.002789	0.002254	0.001445	0.001994	0.0
6	0.0	-0.007055	-0.009688	0.000609	0.001805	0.003116	0.002657	0.001738	0.003046	0.0
7	0.0	-0.031550	-0.028023	0.000398	0.001766	0.003367	0.003065	0.002030	0.007454	0.0
8	0.0	-0.023489	-0.021070	0.000417	0.001390	0.003644	0.003475	0.001949	0.003114	0.0
9	0.0	-0.097979	-0.204160	-0.005354	-0.000911	0.003558	0.003421	0.003248	0.001310	0.0
10	0.0	-0.017045	-0.062027	-0.030089	-0.002985	0.002469	0.003372	-0.001228	-0.004361	0.0
11	0.0	-0.098211	-0.204420	-0.005348	-0.000909	0.003560	0.003421	0.003249	0.001310	0.0
12	0.0	-0.023536	-0.021082	0.000415	0.001392	0.003645	0.003474	0.001949	0.003113	0.0
13	0.0	-0.031517	-0.027893	0.000399	0.001766	0.003366	0.003065	0.002030	0.007449	0.0
14	0.0	-0.007072	-0.009676	0.000608	0.001804	0.003115	0.002657	0.001738	0.003046	0.0
15	0.0	0.002923	0.008029	0.003799	0.001740	0.002789	0.002253	0.001445	0.001994	0.0
16	0.0	0.000490	0.005373	0.004435	0.001473	0.002291	0.001784	0.001153	0.001375	0.0
17	0.0	0.000578	0.004646	0.003867	0.001054	0.001657	0.001254	0.000803	0.000841	0.0
18	0.0	-0.001443	-0.000302	0.001843	0.000804	0.001228	0.001019	0.000736	0.000760	0.0
19	0.0	-0.004808	-0.010774	-0.004998	0.000566	0.001156	0.000923	0.000568	0.000662	0.0

c. $u_2'u_3'$ Shear Stress

U1U1 * E 2

REYNOLD'S STRESS.

1	0.0	0.002512	0.022200	0.035074	0.037133	0.062613	0.058756	0.029549	0.014968	0.0
2	0.0	0.002115	0.016639	0.034382	0.034986	0.058442	0.052343	0.031156	0.014598	0.0
3	0.0	0.002580	0.017736	0.031675	0.034454	0.059128	0.052292	0.029247	0.013989	0.0
4	0.0	0.003276	0.019280	0.033408	0.035589	0.058637	0.050476	0.027791	0.013122	0.0
5	0.0	0.004016	0.019308	0.033597	0.035740	0.058192	0.048750	0.025971	0.012236	0.0
6	0.0	0.004972	0.018264	0.027340	0.036426	0.057213	0.046506	0.023778	0.010994	0.0
7	0.0	0.005324	0.020809	0.022881	0.035851	0.056705	0.046910	0.023167	0.010509	0.0
8	0.0	0.003339	0.017593	0.021438	0.027953	0.054268	0.048686	0.024872	0.011563	0.0
9	0.0	0.009687	0.053322	0.039949	0.044301	0.052643	0.047631	0.023281	0.011985	0.0
10	0.0	0.000946	0.014947	0.100162	0.051176	0.047751	0.046266	0.026695	0.012770	0.0
11	0.0	0.009704	0.053332	0.039954	0.044268	0.052654	0.047630	0.023281	0.011983	0.0
12	0.0	0.003351	0.017597	0.021435	0.027984	0.054284	0.048682	0.024871	0.011562	0.0
13	0.0	0.005333	0.020793	0.022863	0.035855	0.056707	0.046908	0.023168	0.010509	0.0
14	0.0	0.004978	0.018242	0.027318	0.036429	0.057223	0.046506	0.023779	0.010994	0.0
15	0.0	0.004024	0.019293	0.033541	0.035732	0.058208	0.048745	0.025970	0.012236	0.0
16	0.0	0.003282	0.019263	0.033353	0.035569	0.058648	0.050474	0.027794	0.013124	0.0
17	0.0	0.002589	0.017727	0.031602	0.034448	0.059149	0.052287	0.029245	0.013988	0.0
18	0.0	0.002118	0.016634	0.034353	0.034971	0.058454	0.052343	0.031162	0.014600	0.0
19	0.0	0.002511	0.022182	0.035053	0.037117	0.062623	0.058751	0.029551	0.014968	0.0

d. $\overline{u_1'u_1'}$ Normal Stress

Figure 26. Computed Reynolds Stress Distributions (Contd)

U2U2 * E 3

REYNOLD'S STRESS.

1	0.0	0.000150	0.001309	0.002067	0.002222	0.003754	0.003517	0.001764	0.000873	0.0
2	0.0	0.000126	0.000983	0.002043	0.002099	0.003504	0.003133	0.001856	0.000847	0.0
3	0.0	0.000156	0.001073	0.001919	0.002076	0.003555	0.003137	0.001745	0.000808	0.0
4	0.0	0.000200	0.001181	0.002029	0.002145	0.003527	0.003026	0.001652	0.000739	0.0
5	0.0	0.000245	0.001176	0.002032	0.002150	0.003494	0.002917	0.001538	0.000670	0.0
6	0.0	0.000306	0.001115	0.001650	0.002189	0.003429	0.002773	0.001398	0.000557	0.0
7	0.0	0.000341	0.001342	0.001399	0.002174	0.003432	0.002824	0.001369	0.000361	0.0
8	0.0	0.000217	0.001109	0.001308	0.001708	0.003328	0.002975	0.001519	0.000660	0.0
9	0.0	0.000339	0.001753	0.002212	0.002516	0.003124	0.002860	0.001354	0.000922	0.0
10	0.0	-0.009003	-0.014534	0.001227	0.002044	0.002667	0.002804	0.001529	0.001105	0.0
11	0.0	-0.524553	-0.149952	-0.000383	0.001701	0.002880	0.002807	0.001012	0.000254	0.0
12	0.0	-0.435885	-0.085765	-0.000046	0.001485	0.003058	0.002743	0.001442	0.000022	0.0
13	0.0	-0.678674	-0.120457	0.000208	0.001894	0.003219	0.002649	0.001317	-0.002666	0.0
14	0.0	-0.673655	-0.114230	-0.002094	0.001890	0.003286	0.002675	0.001384	0.000011	0.0
15	0.0	-0.577130	-0.150983	-0.020505	0.001648	0.003320	0.002809	0.001502	0.000360	0.0
16	0.0	-0.476509	-0.163241	-0.029327	0.001452	0.003312	0.002892	0.001583	0.000494	0.0
17	0.0	-0.386404	-0.156345	-0.027257	0.001421	0.003325	0.002979	0.001654	0.000584	0.0
18	0.0	-0.296499	-0.138218	-0.029152	0.001441	0.003274	0.002983	0.001759	0.000558	0.0
19	0.0	-0.393627	-0.212133	-0.038651	0.001310	0.003610	0.003441	0.001710	0.000655	0.0

e. $\overline{u_2'u_2'}$ Normal Stress

U3U3 * E 3

REYNOLD'S STRESS.

1	0.0	-0.393516	-0.212302	-0.038689	0.001310	0.003610	0.003442	0.001710	0.000655	0.0
2	0.0	-0.296090	-0.138406	-0.029217	0.001440	0.003274	0.002983	0.001758	0.000557	0.0
3	0.0	-0.385351	-0.156668	-0.027366	0.001419	0.003324	0.002980	0.001654	0.000584	0.0
4	0.0	-0.476073	-0.163557	-0.029399	0.001450	0.003311	0.002892	0.001583	0.000493	0.0
5	0.0	-0.576276	-0.151267	-0.020559	0.001647	0.003319	0.002810	0.001502	0.000360	0.0
6	0.0	-0.673052	-0.114484	-0.002100	0.001890	0.003286	0.002675	0.001384	0.000011	0.0
7	0.0	-0.677799	-0.120654	0.000208	0.001894	0.003219	0.002649	0.001317	-0.002673	0.0
8	0.0	-0.434836	-0.085856	-0.000044	0.001483	0.003057	0.002743	0.001442	0.000022	0.0
9	0.0	-0.524161	-0.150012	-0.000387	0.001701	0.002880	0.002807	0.001013	0.000254	0.0
10	0.0	-0.009019	-0.014542	0.001222	0.002044	0.002667	0.002804	0.001529	0.001105	0.0
11	0.0	0.000339	0.001751	0.002213	0.002514	0.003125	0.002860	0.001354	0.000922	0.0
12	0.0	0.000218	0.001109	0.001307	0.001710	0.003329	0.002975	0.001519	0.000660	0.0
13	0.0	0.000341	0.001341	0.001398	0.002174	0.003432	0.002823	0.001369	0.000361	0.0
14	0.0	0.000306	0.001113	0.001649	0.002189	0.003429	0.002773	0.001398	0.000557	0.0
15	0.0	0.000245	0.001175	0.002029	0.002150	0.003495	0.002916	0.001538	0.000670	0.0
16	0.0	0.000201	0.001179	0.002025	0.002144	0.003527	0.003026	0.001652	0.000739	0.0
17	0.0	0.000156	0.001072	0.001915	0.002076	0.003556	0.003136	0.001745	0.000808	0.0
18	0.0	0.000126	0.000983	0.002042	0.002098	0.003504	0.003133	0.001857	0.000847	0.0
19	0.0	0.000150	0.001308	0.002066	0.002222	0.003754	0.003517	0.001764	0.000873	0.0

f. $\overline{u_3'u_3'}$ Normal Stress

Figure 26. Computed Reynolds Stress Distributions (Conld)

DATA DECK SPECIFICATIONS

Input facilities for the COMOC III computer program are sophisticated and greatly simplify data deck preparation and modification. The program sequentially scans the data deck and operates on command data cards as they are encountered. Numerical data required for each command operation are input in free format on cards directly following the command card. Command operations can cause arrays to be filled, initiate a series of solution operations or specify output formats and titles. Command card sequence is quite flexible and care has been taken to ensure that most operations which must be performed sequentially are specifiable under one command name.

Most numerical data may be input in free format. Data delimiters may be blanks or commas, thus allowing for esthetic and meaningful arrangement of data and simple addition or deletion of interspersed numbers. Several features of free format input which greatly simplify repetitive and sequential data specifications are:

Repetitive Numbers:	12.5*7
Fills Array	12. 7. 7. 7. 7. 7.
Repetitive Sequence (one per card only)	2(5. 2. 4.
Fills Array	5. 2. 4. 5. 2. 4.
Skip P locations	10. 12. 3*P 22. T
Fills Array	10. 12. ▽ ▽ ▽ 22.
Increment by a constant	5*50 10 T
Fills Array	10 60 110 160 210
Exponential Notation	6. 10.0E-2 14.E-4 T
Fills Array	6. .1 .0014

The data deck for a wing-fuselage juncture region solution is segmented into several sections for description, but appears in sequential order as indicated by the line numbers. The data has been lumped into meaningful categories, each of which can be related to the juncture flow problem and/or specific requirements for differential equation solution (eg., initial conditions, boundary conditions, etc.) The Fortran MAIN program contains important dimensioning parameters together with coding which links 3D inviscid interaction data with the viscous solution and is listed following the data deck description.

I NAMELIST (Integer) INPUT

```
 1
 2
 3DPNS
 4ICOND
 5  WING-FUSELAGE JUNCTURE FLOW.
 6FENAME
 7 &NAME01
 8          NODE = 210,     LCOL = 50,      KROW = 50,
 9          NSNODE = 19,    NSELEM = 2,     ISIDE = 4,      NVAR = 3,
10          LG = 32,        NBC = 0,        NWALLS = 4,     NTCHEK = 3,
11          NEQ = 9,        NEQKNN = 5,     NEQADD = -4,    NIZS = 250,
12          NYY = 4,        NZZ = 4,        JORDER = 1,     NBAND = 23,
13          NSPEC = 4,      NVP = 13,       NSTRT = 11,     NDP = 10,
14          NFIX2 = 1,      ITKE = 0,       NDERIV = 2,
15          NPTS = 101,     NDIM = 200,     NSTREP = 1,     NODES = 170,
16          NPVSX = 570,    NDPVSX = 1250,  NPVSXT = 14,    IARRAY(394)=3,
17          NVRHS = 7,                      MLTLHS = 3,     NVRH = 7,
18          TRIDPV = 1,     IARRAY(281)=9048,   0,    60,    62,
19          NPR = 7,        IPHI = 1,       NPRFS = -1,     K8SAV = -1,
20          ICORN = 1,      LPHI = -1,
21          TBL = 1,        N3DPNS = 1,     NMCNTR = 1,     N2WAKE = 0,
22          NMOUT = 2,      NMBOUT = 50,    NC = 8,         NOUTS = 1,
23          NCOMPG = 35,    IDIERT = 30,    NMOL = 8,       NIMPLT = 1,
24          NOUTVC = 10,    KNTPAS = 10,
25          KDUMP = 1,
26 &END
```

Line	Command	
3		Solution Procedure (3D parabolic Navier-Stokes)
5		Data Deck Titles
6	FENAME	Command to initiate Namelist read
8	NODE	Slightly larger than the number of nodes in solution
9	NSNODE	Number of nodes in MACRO element geometry
	NSELEM	Number of macro-elements to be refined
10	LG	Set greater than the total number of one-dimensional node sets specified under command CNTNDS.
	NBC	Number of gradient boundary condition sets
11	NEQ	Number of variable arrays in solution (LISTED following command IPINT)
	NEQKNN	Number of variables being integrated (eg. first 5 listed following IPINT)
	NEQADD	Number of variables not being integrated during first few initializing integration steps.
12	NBAND	Jacobian band width (must be an odd number)

I NAMELIST (Integer) INPUT (contd.)

Line	Command	
14	NE1E2	Turbulence Model Switch 0 - No MLT 1 - MLT 2 - MLT when current station is greater than E1E2SW
	ITKE	Turbulence Model Switch 0 - No TKE (see C4EDSW in NAME02) 1 - 2 eqn. TKE, DISS Model
16	NPVSX	Number of entries in C_p tables (formed)
	NPVSXT	Number of entries in C_p tables (inviscid data)
17	NVRHS	Perturbation pressure variable No. (Parameter arrays must be in order; p_p, p_c, ϕ)
20	ICORN	Set to 1 for juncture region flow
21	NMOUT	Standard print format 2 - Arranged in geometrical shape (some data may be omitted) 3 - Columnar by node number
	NMBOUT	Number of variables to be printed (specified under IOSAV)
	NC	Number of significant figures printed
23	IDIFRT	Debug from WLFLXS (number of times)
24	KNTPAS	Causes print to occur as a function of the pass counter (over-rides DELP)
25	KDUMP	ECHO print of input data

II NAMELIST (Real) INPUT

```
27 &NAMEO2
28          UINF = 300.,    TOFINF = 530., PINF = 2116.8, REFL = 1.0,
29          CON = .41,      COMPX = 2.,    COMPY = 2.,
30          PARRAY(126)=1.,1.0E6,          3*1.0,
31          CE = 1.0,       CW = 1.0,      YPLUS = 30.,
32          YI = 2.0,       BLTH = 0.5,
33          SIMPLT = .01,   CHIEPS = 1.E-5,CHISTP = 10.,  TMULT = 1.44,
34          DSTART = 1.,    E1E2SW=10000., C4EDSW=.C0999, VSTART = 0.,
35          EEMULT=-.002,   HSINIT=1.0E-4,
36          TO = .11,       TD = 0.18,     DELP = 0.,     HMAX = 2.,
37 &END
```

Line	Command	
28	UINF	Velocity non-dimensionalizing factor
	TINF	Temperature non-dimensionalizing factor
	PINF	Pressure non-dimensionalizing factor
29	COMPX	Direction 3 compression factor for geometric form print (NMOUT = 2)
	COMPY	Direction 2 compression factor for geometric form print (NMOUT = 2)
33	SIMPLT	Station at which to switch from explicit to implicit integration.
	CHIEPS	Matrix iteration convergence interval.
	CHISTP	Implicit integration step limit
34	DSTART	
	E1E2SW	Integration station where NE1E2 flag is changed (MLT)
	C4EDSW	Integration station where ITKE flag is changed (TKE)
35	HSINIT	Initial integration step size
36	TO	Initial integration station
	TD	Total integration distance (TF = TO + TD)
	DELP	Integration print interval (% of TD)
	HMAX	Maximum allowable step size

III DYNAMIC ARRAY DIMENSIONING AND DEPENDENT VARIABLE SPECIFICATION

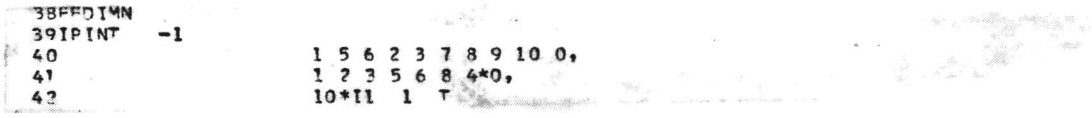

Line	Command	
38	FEDIMN	Dimension arrays to fit problem size
39	IPINT	Cards following specify dependent variables
40		Variable 1 parimary flow velocity
		5 TKE
		6 Dissipation
		2 Transverse velocity (V_2)
		3 Transverse velocity (V_3)
		7 Perturbation pressure (p_p)
		8 Complementary pressure (p_c)
		9 Continuity equation potential[1] (ϕ_1)
41		List of variables which are extrapolated at each new implicit integration station.
42		Variable number assignment

Note: NEQKNN in NAMEO1 specifies the number of integrated differential equations (i.e. the first NEQKNN Variables in Line 40 are integrated).

IV FLOWFIELD GEOMETRY

```
43LINK4     9
44IARRAY    450  250  T
45PSIBD     -1
46                    1  -2  T
47LINK2     14
48NETA
49                    9  9  T
50NEPS
51                    9  9  T
52STYPE
53                    2*4  T
54SELCN
55                    9  10  3  1  12  13  19  2
56                    1  3  14  15  19  16  17  18  T
57DEPVAR     289  290 1248
58              0., .8  .01918   0.  .025  .05  .025  .0  .1731  .1731
59              .2  1.25 .8  .01918   0.  1.25  1.25  1.25  1.25  1.25
60              0.  0.  .01918   .05  0.  .025  .05  .025  0.  .01918
61              0.  .0009  .01918   .1731  .1731  .08  .0009  .09  .0009
62              0. 0. .758 0. 0. .5 .5 0. 0. .783 0. .720 .58 .783 0.
63                    .58 .720 0.  .71   T
64CONE
65READ      5   63   -26
66                    11 1 2,  2  12  11        T  TURN LOWER RIGHT DIAGONALS.
67READ      5   63   -26  918
68                    182 181 171, 171 172 182 T  TURN UPPER LEFT DIAGONALS.
```

Line	Command	
43	LINK4 9	Dimension arrays required for grid generation
45	PSIBD	Input intended diagonal skew of generated elements 1.) Positive Macro-Element No.- right running 2.) Negative Macro-Element No.- left running
47	LINK2 14	Reads discretization data and generates triangular finite elements in each specified Macro-Element
48	NETA	Number of divisions in local coordinate direction (η)
50	NEPS	Number of divisions in local coordinate direction (ε)
52	STYPE	Type Macro-Element 3 = Triangular 4 = Quadrilateral
54	SELCN	Macro-Element nodal connection table
57	DEPVAR	Coordinate and initial values to be distributed (Variables x_3, x_2, and u_1)

IV FLOWFIELD GEOMETRY (Contd.)

Line	Command	
64	DONE	End geometric data. Grid is refined to specification and generated grid and finite element connection tables are stored for reference. x_3 side node data is a geometric progression ratio (λ) where:

$$\varepsilon_{i+1} = \varepsilon_i + (\varepsilon_{i+1} - \varepsilon_i)^{\lambda}$$

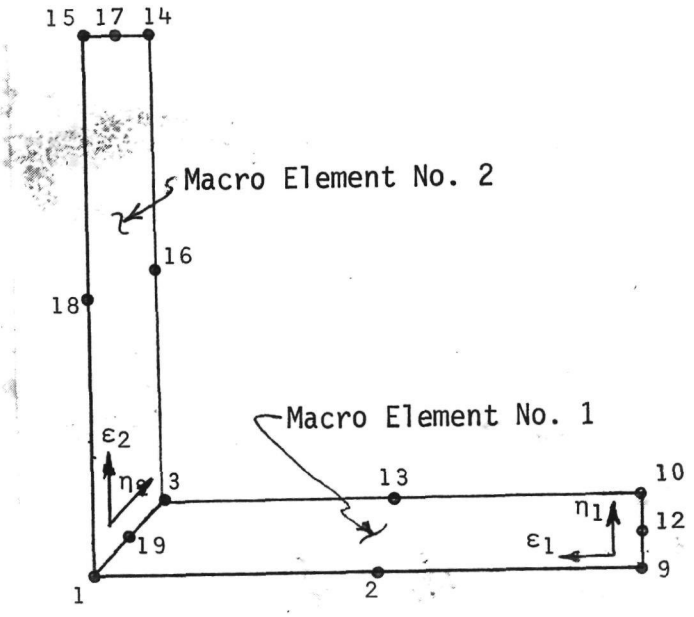

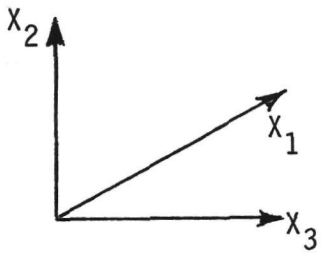

X_1 - Primary Flow Direction

X_2, X_3 - Secondary Flow Plane

V BOUNDARY NODAL ORDERING ARRAYS

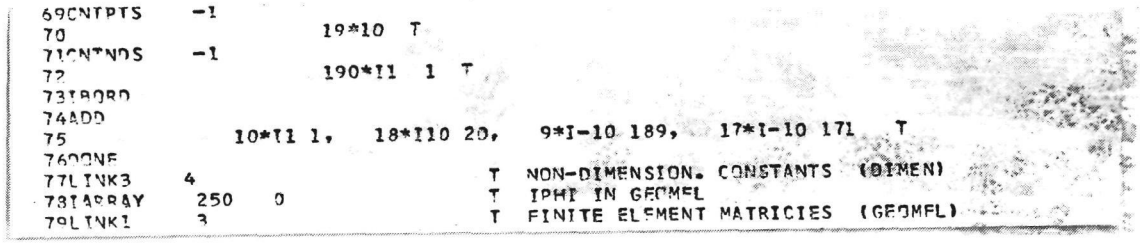

Line	Command	
69	CNTPTS	Number of nodes in each set
71	CNTNDS	Node numbers in each set. Nodes are ordered in sets normal to boundaries of interest
73	IBORD	Sequential numbering of boundary nodes in order parallel to boundaries of interest
77	DIMEN	Form non-dimensionalizing factors
79	GEOMFL	Form Finite Element matrices.

Note: 1) LG in NAMEO1 must be equal to or larger than the total number of sets of data.

2) KWFLXS in NAMEO1 indicates number of sets of this data over which to compute skin friction.

3) LMLT in NAMEO1 is the number of sets of data over which MLT model is used to compute turbulent viscosity.

VI TITLES AND HEADINGS

```
 80DESCRIPT
 81  WING-FUSELAGE JUNCTURE FLOW.
 82DONE
 83COMTITLE
 84  WING-FUSELAGE JUNCTURE FLOW.
 85DONE
 86DESCRIPT  204        T  DESCRIPTIVE TITLE AT BEGINING OF OUTPUT.
 87  WING-FUSELAGE JUNCTURE FLOW.
 88
 89DONE
 90DESCRIPT  332        T  IOPAR  PARAMETER TITLES FOR OUTPUT.
 91 REFERENCE      ENGLISH-FT       ENGLISH-IN        M-K-S            C-G-S
 92 LENGTH.........    .FT.........     .IN.........     .M..........     .CM.........
 93 VELOCITY.......    .FT/S.......     .N.A........     .M/S........     .CM/S.......
 94 DENSITY........    .LBM/FT3....     .N.A........     .KG/M3......     .G/CC.......
 95 TEMPERATURE....    .RANKINE....     .N.A........     .KELVIN.....     .N.A........
 96 ENTHALPY.......    .BTU/LBM....     .N.A........     .KJ/KG......     .N.A........
 97 FROZ.SPEC. HEAT    .BTU/LBM-R..     .N.A........     .KJ/KG-K....     .N.A........
 98 VISCOSITY......    .LBM/FT-S...     .N.A........     .NT-S/M2....     .POISE......
 99 LOCAL PRESSURE     .PSF........     .PSI........     .NT/M2......     .TORR.......
100 LOCAL SOLUTION      .MACH. NO.       ..DPDX1...       ..ENERGY..       .CON. VAR.
101 NWGEOM H'S          ...H21....       ...G22....       ...G23....       ....F1....
102 NWGEOM H'S          ...H31....       ...G32....       ...G33....       ....G1....
103 X1/LREF             .DX1/LREF.       .EPSILON..       .DX1M/LREF REFL REYNOLDS NO
104DONE
105MPARA   -1
106                     5*2,  2*2 162 164 163,  3*2 164 163,  3*2 170 174,
107                     3*2 165 2,  2 -175 3*2,  3*2 176 2,  3*2 177 178,
108                     2 2 169 168 167,  3*2 108 2,  5*2, 5*2, 5*2  T
109IONUMB  -1
110                     999,  5*200,  999,  200 4*43,  200 27 200 2*27,
111                     200 10 200 2*10,  200 58 200 58 200,
112                     200 97 200 97 200,  200 30 200 30 200,
113                     200 38 200 2*38,  999,  39 4*36, 300 154 100 135 122,
114                     200 4*11 186,  200 4*11 139,  11 12 14 85 47   T
115DESCRIPT  203        T  IFMTHD TITLES FOR OUTPUT DEPENDENT VARIABLES.
116 U1/UREF          V2/UREF          V3/UREF          V2PR             V3PR
117PP                PHI1             TKE/TKEREF       DISS/DISSREF     NU/NUREF
118DONE
119IOSAVE  -1
120                     1248  2248  3248  260  262
121                     7248  9248  5248  6248  1247  T
122IOMULT  -1
123                     9*2  21,  10*1  T
124PLOTS    -1
125                     2248  3248  1248              T  U2, U3, U1
```

Line	Command	
83	COMTITLE	Problem identifying titles
86		Std print titles
90		Std output header labels
105	MPARA	Scalar parameter print multipliers
109	IONUMB	Scalar parameter print locations
115		Dependent variable print labels
119	IOSAVE	Dependent variable print locations
122	IOMULT	Dependent variable print multipliers (RARRAY LOC.)

VII DEPENDENT VARIABLE AND PARAMETER BOUNDARY RELATIONS

```
126T
127T --- BOUNDARY CONDITIONS
128T
129KBNO      1
130ADD
131                     19*I10  1    T  FIX WALL NODES.
132DONE
133KBNO      2      1     T  GRADIENT B. C. CARD  0 0 0  A1 2 A3 2
134ADD       0  0  0                 0.  2  0.  2
135                     19*I10  10   T  B. C. ON FREESTREAM NODES.
136ADD
137                     19*I10  1    T  FIX WALL NODES.
138DONE
139KBNO      3      1     T  GRADIENT B. C. CARD  0 0 0  A1 2 A3 2
140ADD       0  0  0                 0.  2  0.  2
141                     19*I10  10   T  B. C. ON FREESTREAM NODES.
142ADD
143                     19*I10  1    T  FIX WALL NODES.
144DONE
145KBNO      5
146ADD
147                     19*I10  1    T  FIX WALL NODES.
148DONE
149KBNO      6
150ADD
151                     19*I10  1    T  FIX WALL NODES.
152DONE
153KBNO      7      1     T  GRADIENT B. C. CARD  0 0 0  A1 2 A3 2
154ADD       0  0  0                 0.  2  0.  2
155                     19*I10  1    T  B. C. ON WALL.
156ADD
157                     9*I1 2,  17*I10 20, 9*I-1 190 T  FIX OUTER BOUNDARY.
158DONE
159KBNO      8
160ADD
161                     9*I1 2,  17*I10 20, 9*I-1 190 T  FIX OUTER BOUNDARY.
162DONE
163KBNO      9
164ADD                  DONE
165                     19*I10  1    T  FIX WALL NODES.
```

Line	Command	
129	KBNO 1	Nodes where U_1 is held constant at initial values (Wall Nodes)
133	KBNO 2	U_2 normal gradient boundary conditions (a_3 internally generated). Followed by nodes where U_2 is held constant.
153	KBNO 7	Perturbation pressure boundary values (internally generated) 1) a_1 = 0.0 indicates symmetry plane boundary 2) a_1 = 1.0 indicates no-slip boundary 3) a_1 = 2.0 indicates slip plane boundary

Note: 1) NBC in NAME01 is set to maximum number of boundary nodes.

VIII TABLE DATA

```
166T
167END          T  ---  3D INVISCID SOLUTION ( FIRST ITERATION ) ---
168T
169T      X         Y          Z                                          CP
170T
171    .107600    0.0        .019180    .999000    .077580    .156600  -.03
172    .107600    .027840    .019180    .999000    .077580    .156600  -.028630      625
173    .107600    .047310    .019190    .991300    .113600    .155400  -.019750      626
174    .107600    .071650    .019180    .991800    .107100    .155400  -.019220      627
175    .107600    .102100    .019180    .995000    .093740    .155900  -.023190      628
176    .107600    .140100    .019180    .999600    .078910    .156700  -.030030      629
177    .107600    .190000    .019180   1.004000    .063880    .157400  -.037850      630
178    .107600    .268700    .019180   1.009000    .047310    .158200  -.045550      631
179    .107600    .418400    .019180   1.012000    .028460    .158600  -.050210      632
180    .107600    .767700    .019180   1.010000    .010420    .158200  -.044320      633
181    .107600   1.516000    .019190   1.004000    .002183    .157400  -.033560      634
182    .107600   3.013000    .019180   1.001000    .000353    .157000  -.027620      635
183    .107600   6.008000    .019180    .998600    .000074    .156500  -.021680      636
184    .107600   9.002000    .019180    .998500    .001582    .156500  -.021550      637
185    .190700    0.0        .030820   1.108000    .061740    .137200  -.265000
186    .190700    .039460    .030820   1.108000    .061740    .137200  -.249200      664
187    .190700    .058910    .030820   1.099000    .100900    .136100  -.235900      665
188    .190700    .087220    .030820   1.094000    .098580    .135600  -.225100      666
189    .190700    .113600    .030820   1.093000    .089010    .135100  -.214700      667
190    .190700    .151600    .030820   1.087000    .076350    .134700  -.205400      668
191    .190700    .201400    .030820   1.084000    .062100    .134300  -.197100      669
192    .190700    .280000    .030820   1.081000    .045330    .133900  -.187900      670
193    .190700    .429600    .030820   1.075000    .026180    .133300  -.175100      671
194    .190700    .778500    .030820   1.067000    .008928    .132200  -.156500      672
195    .190700   1.526000    .030820   1.060000    .001769    .131300  -.140500      673
196    .190700   3.022000    .030820   1.056000    .000281    .130900  -.133100      674
197    .190700   6.012000    .030820   1.054000    .000059    .130600  -.128200      675
198    .190700   9.003000    .030820   1.053000    .001325    .130500  -.125900      676
199    .290800    .0         .041190   1.191000    .041440    .099540  -.442         703
200    .290800    .049830    .041190   1.191000    .041440    .099540  -.429600      703
201    .290800    .069250    .041190   1.183000    .073830    .098910  -.415500      704
202    .290800    .093540    .041190   1.176000    .073420    .098310  -.398200      705
203    .290800    .123900    .041190   1.168000    .067450    .097630  -.378300      706
204    .290800    .161800    .041190   1.159000    .058860    .096910  -.357100      707
205    .290800    .211600    .041190   1.150000    .048500    .096140  -.334500      708
206    .290800    .290200    .041190   1.139000    .035500    .095220  -.308000      709
207    .290800    .439500    .041190   1.126000    .020150    .094080  -.276000      710
208    .290800    .788100    .041190   1.110000    .006504    .092810  -.241500      711
209    .290800   1.535000    .041190   1.101000    .001227    .092000  -.219800      712
210    .290800   3.029000    .041190   1.097000    .000192    .091690  -.211600      713
211    .290800   6.016000    .041190   1.095000    .000040    .091510  -.206800      714
212    .290800   9.004000    .041190   1.093000    .000548    .091380  -.203400      715
213VU2POS            -3                T  VAR. GEOM TABLE STATIONS (X1)
214                    .00999 .0194 .03126 .04628 .06409
215                    .08459 .1076 .1331 .1609 .1907 .2224
216                    .2559 .2908 .3271 .3644 .4025 .4413 .4804  T
217VU2VAL     -3                     T  VAR. GEOM. X2 TABLE
218                    .173 .17478 .177075 .1798 .183 .1865 .1902
219                    .1941 .198 .2018 .2055 .2090 .2122 .2150
220                    .2173 .2191 .2203 .22088   T
221VU3POS            -3                T  VAR. GEOM.  TABLE STATIONS (X1)
222                    .00999 .0194 .03126 .04628 .06409
223                    .08459 .1076 .1331 .1609 .1907 .2224
224                    .2559 .2908 .3271 .3644 .4025 .4413 .4804  T
225VU3VAL     -3                     T  VAR. GEOM.  X3 TABLE
226                    .173 .17478 .177075 .1798 .183 .1865 .1902
227                    .1941 .198 .2018 .2055 .2090 .2122 .2150
228                    .2173 .2191 .2203 .22088   T
```

Line	Command	
167	END	Returns to Main and C_p table data is read.
121-212		3D Inviscid C_p solution and coordinates
213	VU2POS	Coordinates in the primary flow direction where x_2 variation is specified (non-dimensionalized by ALC)

VIII TABLE DATA (Contd.)

Line	Command	
217	VU2VAL	f_2 at each x_1 coordinate followed by f_1 at each x_1 coordinate
221	VU3POS	Same as for VU2POS (x_3 direction)
225	VU3VAL	Same as for VU2VAL (x_3 direction)

IX SOLUTION INITIATION

Line	Command	
229	LINK2 30	Sets up p_C tables
230	LINK1 11	Evaluates p_C from tables at initial station TO
232	LINK2 10	Generates U_1 initial distribution from Cole's Law and p_C array.
233-240	LINK	Initialize other parameters
241	LINKCALL	Parameter evaluation at each integration step.
		1 11 Evaluate p_C this step
		2 4 Evaluate second-order du/dx
		2 15 Evaluate flow integral parameters
		2 3 Evaluate wall shear stresses
		5 6 Evaluate turbulent diffusion coefficients
		5 5 Evaluate perturbation pressure (p_p)
243	QKNINT	Initiate integration of dependent variables
244	EXIT	STOP

X FORTRAN MAIN PROGRAM

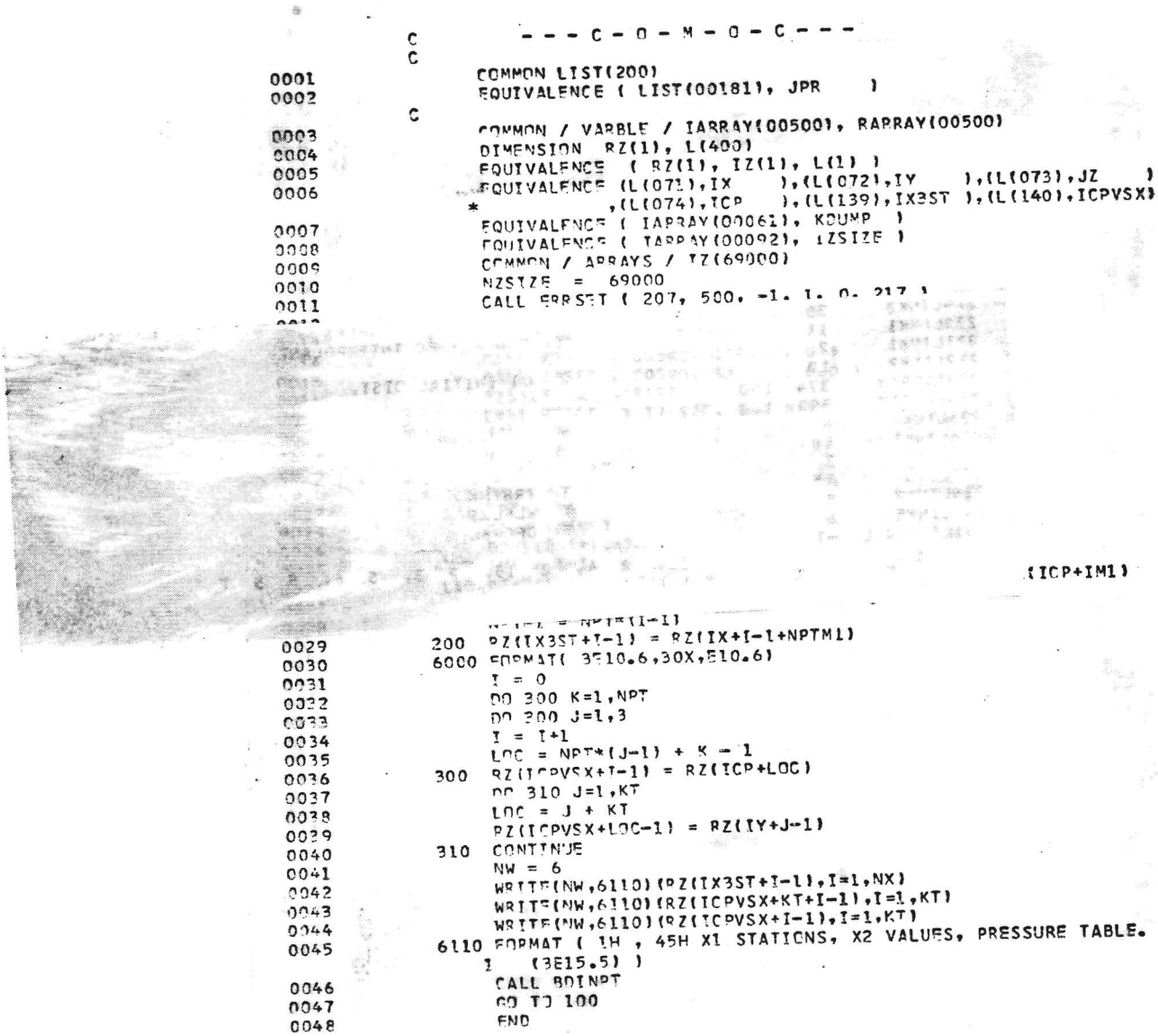

```
C       - - - C - O - M - O - C - - -
C
0001        COMMON LIST(200)
0002        EQUIVALENCE ( LIST(00181), JPR    )
C
0003        COMMON / VARBLE / IARRAY(00500), RARRAY(00500)
0004        DIMENSION  RZ(1), L(400)
0005        EQUIVALENCE  ( RZ(1), IZ(1), L(1) )
0006        EQUIVALENCE (L(071),IX    ),(L(072),IY    ),(L(073),JZ    )
*                      ,(L(074),ICP   ),(L(139),IX3ST ),(L(140),ICPVSX)
0007        EQUIVALENCE ( IARRAY(00061), KOUNP  )
0008        EQUIVALENCE ( IARRAY(00092), IZSIZE )
0009        COMMON / ARRAYS / IZ(69000)
0010        NZSIZE  =  69000
0011        CALL ERRSET ( 207, 500, -1, 1, 0, 217 )
                                                              (ICP+IM1)
0029      200  RZ(IX3ST+I-1) = RZ(IX+I-1+NPTM1)
0030      6000 FORMAT( 3E10.6,30X,E10.6)
0031           I = 0
0032           DO 300 K=1,NPT
0033           DO 300 J=1,3
0034           I = I+1
0035           LOC = NPT*(J-1) + K - 1
0036      300  RZ(ICPVSX+I-1) = RZ(ICP+LOC)
0037           DO 310 J=1,KT
0038           LOC = J + KT
0039           RZ(ICPVSX+LOC-1) = RZ(IY+J-1)
0040      310  CONTINUE
0041           NW = 6
0042           WRITE(NW,6110)(RZ(IX3ST+I-1),I=1,NX)
0043           WRITE(NW,6110)(RZ(ICPVSX+KT+I-1),I=1,KT)
0044           WRITE(NW,6110)(RZ(ICPVSX+I-1),I=1,KT)
0045      6110 FORMAT ( 1H , 45H X1 STATIONS, X2 VALUES, PRESSURE TABLE.      /
              1    (3E15.5) )
0046           CALL BOINPT
0047           GO TO 100
0048           END
```

Line (ISN)

3	Comman block for scalar arrays (Integer, Real)
9	Common block for variable arrays
10	Set program arrays size indicated equal to IZ array dimension
13-16	Initialize all arrays to zero
19	Begin reading data deck (return upon encountering command END)
20-44	Read and store inviscid table data
45	Continue reading data deck commands
46	Begin new problem (terminates with command EXIT)

SUMMARY

A parabolized three-dimensional partial differential equation system has been derived for prediction of turbulent subsonic aerodynamic flows in juncture regions. A Reynolds stress constitutive equation is applied which introduces source terms into the transverse plane momentum equations. These terms depend primarily upon the shear of the axial velocity, and the levels of turbulent kinetic energy and isotropic dissipation. They exert a dominant influence on the momentum equation solutions. The developed 3DPNS equation system and implicit solution algorithm have been coded and evaluated using the COMOC III computer program, and satisfactory performance has been achieved. The 3DPNS equation system, upon pressure coupling within an iterative interaction solution with a three-dimensional potential flow code, can provide a computational methodology for determination of juncture region geometry influences on flow structure and induced drag.

REFERENCES

1. Carrier, G. F., "The Boundary Layer In A Corner," Quart. Appl. Math., Vol. 4, p. 367-378, 1947.

2. Rubin, S. G., "Incompressible Flow Along A Corner," J. Flu. Mech., Vol. 26, Pt. 1, p. 97-110, 1966.

3. Pal, A. and Rubin, S. G., "Asymptotic Features Of Viscous Flow Along A Corner," Q. Appl. Math., Vol. 27, p. 99-108, 1971.

4. Rubin, S. G. and Grossman, B., "Viscous Flow Along The Corner: Numerical Solution Of The Corner Layer Equations,: Q. Appl. Math., Vol. 29, No. 2, p. 169-186, 1971.

5. Weinberg, B. C. and Rubin, S. G., "Compressible Corner Flow," J. Flu. Mech., Vol. 56, Pt. 4, p. 753-774, 1972.

6. Ghia, K. N. and Davis, R. T., "A Study Of Compressible Potential And Asymptotic Viscous Flows For Corner Regions," AIAA J., Vol. 12, No. 3, p. 355-359, 1974.

7. Ghia, K. N. and Davis, R. T., "Corner Layer Flow: Optimization Of Numerical Method Of Solution," Computers and Fluids, Vol. 2, p. 17-34, 1974.

8. Ghia, K. N., "Streamwise Flow Along An Unbounded Corner," AIAA Paper No. 74-559, 1974.

9. Tokuda, N., "Viscous Flow Near A Corner In Three Dimensions," J. Flu. Mech., Vol. 53, Pt. 1, p. 129-148, 1972.

10. Zamir, M. and Young, A. D., "Experimental Investigation Of The Boundary Layer In A Streamwise Corner," J. Aero. Quarterly, Vol. 21, p. 313-339, 1970.

11. Bragg, G. M., "The Turbulent Boundary Layer In A Corner," J. Flu. Mech., Vol. 36, Pt. 3, p. 485-503, 1969.

12. Eichelbrenner, E. A. and Preston, J. H., "On A Role Of Secondary Flow In Turbulent Boundary Layers In Corners (and Salients)," J. deMecanique, Vol. 10, No. 1, p. 91-112, 1971.

13. Gessner, F. B., "The Origin Of Secondary Flow In Turbulent Flow Along A Corner," J. Flu. Mech., Vol. 58, Pt. 1, p. 1-25, 1973.

14. Hess, J. L., "Calculation of Potential Flow About Arbitrary Three-Dimensional Lifting Bodies," Report MDC J5679-01, 1972.

15. Cebeci, T. and Smith, A.M.O., Analysis of Turbulent Boundary Layers, Academic Press, New York, 1974.

16. Lumley, J. L., "Toward A Turbulent Constitutive Relation," J. Flu. Mech., V. 41, Pt. 2, pp. 413-434, 1970.

17. Launder, B. E., Reece, G. J. and Rodi, W., "Progress In The Development Of A Reynolds-Stress Turbulence Closure," J. Flu. Mech., V. 68, Pt. 3 pp. 537-566, 1975.

18. Gessner, F. B., and Emery, A. F., "A Reynolds Stress Model For Turbulent Corner Flows - Pt. I: Development Of The Model,: J. Flu. Engr., Trans. ASME, pp. 261-268, 1976.

19. Hanjalic, K. and Launder, B. E., "A Reynolds Stress Model Of Turublence And Its Application To Thin Shear Flows,: J. Flu. Mech., V. 52, Pt. 4, pp. 609-638, 1972.

20. Briley, W. R., "Numerical Method For Predicting Three-Dimensional Steady Viscous Flow In Ducts, : J. Comp. Phys., 14, pp. 8-28, 1974.

21. Dodge, P. R. "A Numerical Method For 2-D and 3-D Viscous Flows," AIAA Paper 76-425, 1976.

22. Baker, A. J., Finite Element Computational Fluid Mechanics, University of Tennessee, Manuscript, 1978.

23. Soliman, M. O. and Baker, A. J., "A High Order Accurate Numerical Solution Algorithm For Turgulent Boundary Layer Flow," AIAA Paper No. 79-0001, 1979.

APPENDIX

The 3DPNS option in COMOC III is implemented using linear interpolation polynomials spanning triangular-shaped planar finite element domains possessing vertex node points. The basic geometry is illustrated in Figure A.1 including the various coordinate systems employed to span R^2 and R_e^2. The normalized, linearly-dependent coordinate system ς_i is the fundamental descriptor for R_e^2 spanned by linear functions; hence (ref. 22)

$$\{N_1(x_\ell)\} = \{\varsigma(\eta_\ell)\} \tag{A.1}$$

and $k \equiv 1$ in equation (64).

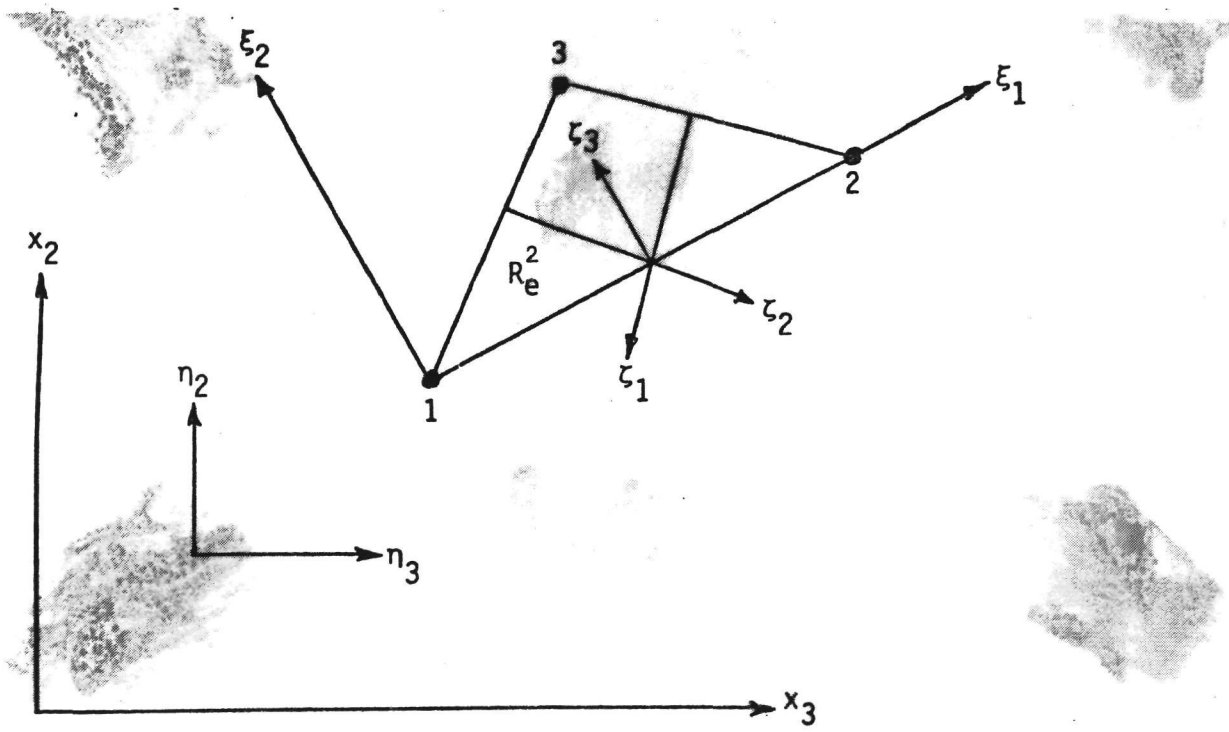

Figure A.1 Coordinate Systems for Two-Dimensional Finite Element

The ζ and η coordinates are related as

$$\{\zeta\} = \begin{Bmatrix} 1 - \xi_1/\xi_1(2) - \left(1 - \xi_1(3)/\xi_1(2)\right)\xi_2/\xi_2(3) \\ \xi_1/\xi_1(2) - \left(\xi_1(3)/\xi_1(2)\right)\xi_2/\xi_2(3) \\ \xi_2/\xi_2(3) \end{Bmatrix} \tag{A.2}$$

where $\zeta_i(n)$ is the i^{th} coordinate pair of node n. Furthermore,

$$\xi_i = a_{ij}\eta_j \tag{A.3}$$

where the elements of a_{ij} are the direction cosines of the coordinate transformation that aligns ξ_1 with the line connecting the first two nodes of R_e^2.

The gradient vector operation is fundamental to the formulation of the equivalent matrix structure. Using the chain rule and the summation convention,

$$\frac{\partial}{\partial x_\ell}\{N(x_\ell)\} = \frac{\partial}{\partial \xi_i}\{\zeta\}\frac{\partial \xi_i}{\partial \eta_k}\frac{\partial \eta_k}{\partial x_\ell} \tag{A.4}$$

The coordinate transformations, equations (A.4) and (48) facilitate the final two evaluations. The gradient operator on ξ_i is an elementary analytical operation using equation (A.2). Derivatives on x_1, see equation (48), introduce additional contributions.

The second calculus operation intrinsic to the algorithm is integration of products of the elements of $\{N_1(x_\ell)\}$ over R_e^2. For example, in the primary mean momentum equation (25), the i = 1 convection term corresponds to f_2 in the general description, equation (60), for q identified with $\tilde{u}_1$. Assuming for simplicity that variable geometry spans only the x_2 coordinate, i.e., $f_{3i} = \{0\}$ in equation (49) this term becomes

$$\bar{\rho}\tilde{u}_1\frac{\partial \tilde{u}_1}{\partial x_1} = \bar{\rho}\tilde{u}_1\left[\frac{\partial}{\partial \eta_1} - (h_{22} + \eta_2 h_{23})\frac{\partial}{\partial \eta_2}\right]\tilde{u}_1 \tag{A.5}$$

Inserting equation (A.5) into the algorithm formulation, equation (65), and using the elemental interpolation for both $\bar{\rho}\tilde{u}_1$ and $\tilde{u}_1$ on R_e^2, and upon rearrangement of scalars, the algorithm equivalent of equation (A.5) is

$$\int_{R_e^2} \{RHOU1\}_e^T \{N\} \{N\} \left[\{N\}^T \{RHOU1\}_e' - \left(h_{22} + h_{23} \{N\}^T \{ETA2\}_e \right) \frac{\partial}{\partial \eta_2} \{N\}_e^T \{RHOU\}_e \right] d\tau \qquad (A.6)$$

Recall that only the elements of $\{N_1\}$ are functions of η, and that the derivative of these linear functions are constants on R_e^2.

Generalizing to $1 \leq j \leq 3$, formation of the finite element equivalent of the three-dimensional convection term in equations (25)-(29) requires directional derivatives. Hence, equation (A.4) becomes

$$\frac{\partial}{\partial x_\ell} \{N(x_\ell)\}_e \equiv h_{21}(x_1) \{B112\}_e \hat{\varepsilon}_2 + h_{31}(x_1) \{B113\}_e \hat{\varepsilon}_3 \qquad (A.7)$$

where the (fixed) coordinate transformation, equation (A.3) is imbedded into the {B11J}. J is the index synonymous with $\hat{\varepsilon}_j$, the unit vectors of x_j, and the elements of {B11J} are independent of x_1.[J] Using these concepts and notation, the linear interpolation finite element equivalent of the entire three-dimensional convection term imbedded in each of the 3DPNS equations as represented within f_i of the general differential equation (60) becomes

$$\int_{R_e^2} \{N\}\bar{\rho}\tilde{u}_i \frac{\partial q}{\partial x_i} d\tau = A_e \Big\{ \Big(\{RHOU1\}_e^T [B3000] \Big) \{Q\}_e$$

$$+ [B200] \Big(\{RHOU2\}_e - g_{22}\{RHOU1\}_e \Big) h_{21} \{B112\}_e^T \{Q\}_e$$

$$+ [B200] \Big(\{RHOU3\}_e - g_{32}\{RHOU1\}_e \Big) h_{31} \{B113\}_e^T \{Q\}_e$$

$$- \Big(\{RHOU1\}_e^T [B3000] \Big) \Big(g_{23}\{ETA2\}_e h_{21} \{B112\}_e^T \{Q\}_e$$

$$+ g_{33}\{ETA3\}_e h_{31} \{B113\}_e^T \{Q\}_e \Big) \Big\} \qquad (A.8)$$

The elements of {ETAJ} are corresponding nodal coordinates of R_e^2. Matrices with second index >2 are hypermatrices, elements of which are themselves matrices, see reference 22, and inner products must be performed in the correct sequence.

The finite element form for the equation determining particular pressure distribution warrants comment. From equation (43), and enforcing the continuity equation (24) directly, imbedding the resultant statement within the finite element algorithm, equation (65), and performing select integrations by parts, yields the following statement for particular pressure $p_p(x_\ell; x_1)$.

$$S_e \Bigg[-\int_{R_e^2} \frac{\partial \{N\}}{\partial x_\ell} \frac{\partial p_p}{\partial x_\ell} d\tau + \int_{R_e^2} \{N\} \frac{\partial \bar{\rho}\tilde{u}_j}{\partial x_\ell} \frac{\partial \tilde{u}_\ell}{\partial x_j} d\tau + \int_{R_e^2} \frac{\partial \{N\}}{\partial x_j} \tilde{u}_j \left[\frac{\partial \bar{\rho}}{\partial x_\ell} \tilde{u}_\ell + \frac{\partial (\bar{\rho}\tilde{u}_1)}{\partial x_1} \right] d\tau$$

$$- \int_{\partial R_e^2 \cap \partial R_e^2} \{N\} \left[\rho \tilde{u}_j \frac{\partial \tilde{u}_\ell}{\partial x_j} - \frac{\partial}{\partial x_k} \left(\mu e \left[\frac{\partial \tilde{u}_\ell}{\partial x_k} + \frac{\partial \tilde{u}_k}{\partial x_\ell} \right] \right) \right] \hat{n}_\ell d\tau$$

$$- \oint_{\partial \Omega_e} \{N\} \left[\frac{\partial \bar{\rho}}{\partial x_\ell} \tilde{u}_\ell + \frac{\partial (\bar{\rho}\tilde{u}_1)}{\partial x_1} \right] \tilde{u}_j \hat{n}_j \, d\tau \Bigg] \equiv \{0\} \qquad (A.9)$$

Equation (A.9) employs the limited summation convention, $1 \leq i, j \leq 3$, and $2 \leq k, \ell \leq 3$, and equations (A.4) and (47) must be employed in the matrix development to replace derivatives on x_1. Note in particular that $\partial\{N_1\}/\partial x_1$ does not vanish identically in the variable juncture geometry.

The first term in equation (A.9) is the Laplacian operator written on particular pressure. The second and third terms result from an integration by parts of the second term in the parent equation (43), and simplification using the continuity equation (24). The fourth term is the boundary condition statement, equation (42), and valid on symmetry plane, no-slip and slip-wall closure segments. The last term is a closed surface integral over an x_1 integration step, resulting from use of a Green-Gauss theorem in the integration by parts. Since $\tilde{u}_j \hat{n}_j$ vanishes on all closure segments ∂R_e^2 for confined flow, this term involves an integration over R_e^2 at the current station, followed by subtraction of the previous station evaluation on an assembled basis.

Since the convection and boundary condition terms in equation (A.9) involve double summation index sets, the resultant expansions in transformed coordinates are very lengthy. Nevertheless, upon application of the finite element interpolation, equation (64), employing the developed standard matrix forms, and combining like terms, each of the integral expressions can be directly evaluated on a triangular non-regular discretization of R^2. For example, for coordinate stretching spanning x_2 only, and recalling that $1 \leq j \leq 3$ includes initial-value derivatives on x_1, the second term in equation (A.9) (9.9) becomes,

$$\int_{R_e^2} \{N\} \frac{\partial \bar{\rho}\tilde{u}_j}{\partial x_\ell} \frac{\partial \tilde{u}_\ell}{\partial x_j} d\tau = A \Bigg[$$

$$\{RHOU1\}_e^T \{B112\}_e h_{21} \Big([B200]\{U2\}_e' - g_{22}\{B10\} - g_{23}[B200]\{ETA2\}_e \Big) h_{21} \{B112\}_e^T \{U2\}_e$$

$$+ \{RHOU1\}_e^T \{B113\}_e \Big([B200]\{U3\}_e' - g_{22}\{B10\} - g_{23}[B200]\{ETA2\}_e \Big) h_{21} \{B112\}_e^T \{U3\}_e$$

$$+ \{B10\} \Big[\{RHOU2\}_e^T \{B112\}_e h_{21}^2 \{B112\}_e^T \{U2\}_e + \{RHOU3\}_e^T \{B113\}_e^T \{B113\}_e^T \{U3\}_e$$

$$+ 2 \Big(\{RHOU2\}_e + \{U2\}_e \Big) \{B113\}_e h_{21} \{B112\}_e^T \Big(\{U3\}_e + \{RHOU3\}_e \Big) \Big] \Bigg] \qquad (A.10)$$

Equation (A.10) is a column matrix of degree three, and the matrices with superscript prime denote the nodal distribution of x_1-derivatives of the corresponding dependent variable. The coding of the PPRES subroutine in COMOC III, for evaluation and solution of equation (A.9), contains terms written in the formalism exhibited in equation (A.10).

1. Report No.	2. Government Accession No.	3. Recipient's Catalog No.
NASA CR-159024		

4. Title and Subtitle	5. Report Date
Numerical Prediction of Turbulent Three-Dimensional Juncture Region Flow Using The Parabolic Navier-Stokes Equations	October, 1978
	6. Performing Organization Code: CoMoC 78TR-3
7. Author(s): A. J. Baker, P.D. Manhardt & J.A.Orzechowski	8. Performing Organization Report No.
9. Performing Organization Name and Address: Computational Mechanics Consultants, Inc. 3601-A Chapman Hwy. Knoxville, TN 37920	10. Work Unit No.
	11. Contract or Grant No.: NAS1-15105
12. Sponsoring Agency Name and Address: National Aeronautics & Space Administration Washington, DC 20546	13. Type of Report and Period Covered: Contractor Report
	14. Sponsoring Agency Code

15. Supplementary Notes

Langley Technical Monitor: Douglas L. Dwoyer

Final Report

16. Abstract

A numerical solution algorithm is established for prediction of subsonic turbulent three-dimensional flows in aerodynamic configuration juncture regions. In concert with a full three-dimensional exterior potential flow solution, the developed parabolic algorithm yields prediction of the details of the corner region flows. A turbulence closure model is established using the complete Reynolds stress. Pressure coupling is accomplished using the concepts of complementary and particular solutions to a Poisson equation. Numerical results are presented for prediction of the three-dimensional turbulent flow in the juncture of two intersecting parabolic arc airfoils. Specifications for data input requirements for COMOC III are discussed.

17. Key Words (Selected by Author(s))	18. Distribution Statement
Wing-Body Juncture Flow Turbulent Three-Dimensional Parabolic Navier-Stokes	Unclassified Unlimited

19. Security Classif. (of this report)	20. Security Classif. (of this page)	21. No. of Pages	22. Price*
Unclassified	Unclassified	69	

*For sale by the Clearinghouse for Federal Scientific and Technical Information, Springfield, Virginia 22151.